UNIVERSITÀ DEGLI STUDI DI PADOVA
Department of Agronomy Food Natural Resources Animals and Environment
and
Department of Land, Environment Agriculture and Forestry

Second Cycle Degree (MSc)
in
SUSTAINABLE AGRICULTURE

Three-dimensional quantitative characterization of grapes morphology and possible relation with grey mould susceptibility

Supervisor
Prof. Francesco Marinello

Co-supervisor
Dott. Alessandro Zanchin

Submitted by
Mahshid Kalantari
Student no. 2004960

ACADEMIC YEAR 2022-2023

Table of Contents

Abstract

Grey mould is one of the most important diseases of grapevine in the Mediterranean regions caused by the fungi *Botrytis cinerea*. Many factors are responsible for this disease among them, the morphology of grapes plays a crucial role in grey mould infection. The grapes with highly compact berries are the most susceptible to infection. The common methods applied to evaluate the compactness of grapes cannot apply to grapevine bunches from the same variety. Therefore, novel methods are used to detect compactness by image processing analyses such as photogrammetry for 3D model reconstruction.

This study proposes an alternative analysis of bunch morphology and compaction assessment based on virtual 3D models. Seventeen Pinot Gris clones and six Pinot Noir clones were manually collected at harvest time, and the grey mould severity evaluation was carried out in the field. All the grapes were photographed at different angulations, and the 3D model reconstruction was performed by the photogrammetry technique. Several measures and indexes were extracted from each bunch. Principal component analysis (PCA) and two multiple linear regression models (MLR) were applied to identify the descriptors of the clones most related to grey mould infection. The first model assessed the correlation between the grey mould severity and the descriptors from the 2D analysis, while the second model analyzed both descriptors from the 2D and 3D analysis. The 3D MLR presented higher performances than the 2D MLR. The R-square value (R^2) and the root mean square error (RMSE) were compared between models. For Pinot Gris, the R^2 rose from 0.656 to 0.838, moving from the 2D to the 3D MLR, while the RMSE decreased from 1.713 to 1.175. In Pinot Noir, the 2D model did not provide sufficient robustness, while the proposed MLR estimated R^2 with 0.936 value and RMSE with 0.29 value. Additional studies were performed by analyzing the data with graphs and statistics. Consequently, the most significant traits include the estimated empty volume, the width of the grape, weight, volume, shape, and the ratio between surface and height.

Keywords: Photogrammetry, Bunch compactness, Bunch morphology, Grey mould, Optical sensors.

Chapter 1
Introduction

1.1. The Importance of Viticulture in the World and Italy

Grape is one of the most important fruits globally, especially as a produced fruit crop. Around 50% of grapes are transformed and consumed as wine, one-third of grapes are used as fresh fruit, and the rest is dried (International Organisation of Vine and Wine. 2016).

Viticulture could be an agricultural activity that is typically more profitable per area than annual crops. Several cultivars of red and white grapes are grown for fresh consumption or for producing wines, juice, and raisins (Brunetto et al. 2020). Viticulture is the broad term for the cultivation, protection, and harvest of grapes where the operations are outdoors (Chandrasekar Venkitasamy 2019). Viticulture is possible in both subtropical regions and colder temperate areas. The major problem in moist subtropical regions is controlling diseases and it is recommended to prune to promote bud burst for continued growth. In a cold climate, it is required to adapt varieties to avoid the breaking of endogenous dormancy during the cold winter weather (Jackson 2016).

The cultivation area of the world grapes was almost 7.5 million hectares in 2018. Five countries deputed about 50% of the world's vineyards and 9% of this percentage belonged to Italy (705000 ha). Approximately 77.8 mt (millions of tons) of grapes were produced in the world in 2018 and about 57% of this number appertains to wine grapes. Italy was the first country as a wine producer in the world with 54.8 million hectoliters of wine grape production and the third country as a wine consumer with a rate of 22.4 hectoliters in 2018. In addition, Italy had a second place as a wine exporter with a proportion of 19.7 million hectoliters (International Organization of Vine and Wine Intergovernmental Organization (OIV) 2019).

1.2. Importance of varieties

1.2.1. Pinot Gris

Pinot Gris is an important variety of wine grapes in Italy and its cultivation area is about 25000 ha, about 3.7% of this country's total vineyard cultivation area. The trend of growing this variety is increasing which has expanded its area by 35% in 5 years in Italy and made it the fourth Italian variety that is cultivated (International Organization of Vine and Wine Intergovernmental (OIV) 2017).

According to the latest Veneto Agricoltura report related to the regional wine sector, there is a constant increase in the area planted with vines and wine exports (2.22 billion / € in 2018) for Prosecco and Pinot Gris. This constant increase is due mostly to Pinot Gris (+132.6%) and another variety called Glera (+167%). PDO DELLE VENEZE is the most important PDO labeling for Pinot Gris grapes and wines in the Veneto region. The total amount of Pinot Gris grapes produced in Veneto from 2016 to 2020 is growing from 131000 tons to 179400 tons (Veneto Agricoltura. 2019).

About half of Pinot Gris production in the world comes from Italy, where 85% is concentrated in the North-East of Italy area and almost ten thousand winemakers in Trento Province, Veneto, and Friuli Venezia Giulia. It seems that over 31000 hectares are covered with Pinot Gris cultivated in Italy, of which 27000 are in the North-East of Italy (under the PDO delle venezie) (Unione Italiana Vini 2020)

Pinot Gris is a white wine grape variety of the species *Vitis vinifera*. It is thought to be a mutant clone of the Pinot Noir grape; in Italy, it is known as "Pinot Grigio". The name "Pinot" refers to the French word "pinecone" because the grapes grow in small pinecone-shaped clusters. The wines produced from this grape also vary in color from a deep golden yellow to copper and even a light shade of pink, and it is one of the more popular grapes for orange wine (Robinson 1986).

1.2.2. Pinot Noir

Pinot Noir is another important grape variety, which its cultivated area is about 112000 ha, in Italy and it has a growing trend in production. It is an early-budding variety that is sensitive to early spring frosts but is resistant to winter frosts. As a result, not only could

it be widely grown in European countries, such as Germany, Italy, Switzerland, Romania, Hungry, and Spain, but also in the vineyards of New World countries, including the United States, New Zealand, Australia, Chile, Argentina, and South Africa. It ripens quickly in warm climates. Pinot Noir grapes are susceptible to *Botrytis cinerea*. It has small clusters and very small berries that produce low yields. Although its grapes are high in sugar and moderately acidic, their skin is rich in polyphenols. It produces lightly colored wines that are popular with consumers and has a good potential for aging in barrels. It ranks as the world's fourth most cultivated variety of wine grapes (International Organization of Vine and Wine Intergovernmental (OIV) 2017).

1.3. The fungal disease

1.3.1. Grey Mould

Grey mould is one of the most important diseases of grapevine in temperate climates. *Botrytis cinerea* is a polyphagous saprophytic pathogen that can cause this disease in more than 1400 species of cultivated plants (Elad 2016). It makes massive losses in some fields- and greenhouse-grown horticultural crops before harvest, or even at the seedling stage in some hosts (Staats et al. 2005). *Botrytis cinerea* is responsible for significant economic loss in vineyards worldwide (P. A.G. Elmer and Reglinski 2006). It can make off-flavors, unstable color, oxidative damage, premature aging, and difficulties in clarification in wine. Furthermore, other pathogens like bacteria and fungi could invade infected clusters and exacerbate plant disease (D Molitor et al. 2011).

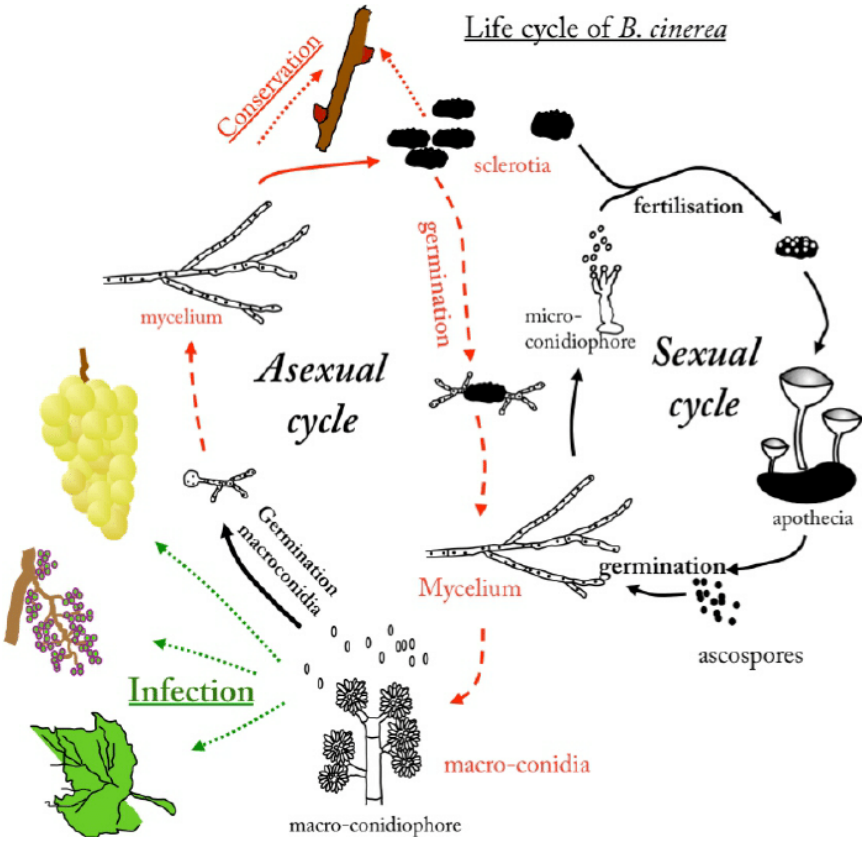

Figure 1.1. Life cycle of *Botrytis cinerea* on grape (Billard et al. 2011).

Botrytis cinerea is known as a pathogen for many crops both pre and postharvest. It can develop from rotted fruit next to healthy fruit, causing the extensive breakdown of the commodity, and sometimes spoiling entire lots. The pathogen can progress infections at storage temperatures (usually 0–5°C) when fruit resistance is decreased. *B. cinerea* is the only species in the genus with a broad host range and it has two stages in its life cycle: the sexual and asexual stages as shown in Figure 1.1.

The fungus exists in different forms such as mycelia, micro- and macroconidia, chlamydospores, sclerotia, apothecia, and ascospores, and they are dispersed by diverse means. In the vegetative stage, mycelium produces asexual conidia (macroconidia) and in undesirable environmental conditions, it produces sclerotia. Sclerotia usually germinate to produce mycelium or conidia, but after appropriate conditions and fertilization, they may germinate to produce aphotecia (teleomorph stage), containing ascospores resulting from meiosis but this stage is very rare. In temperate climates, the sclerotia germinate in

spring as a primary source of inoculum within a crop. In addition, during winter and in times that are not favourable for the fungus, sclerotia and mycelium of *B. cinerea* survive within infected dead host tissues left as crop debris, plant weeds, and inside some seeds as primary inoculum. In perennial crops, the dead leaves, flowers, and mummified fruits contain masses of mycelium that can often be ideally situated within a crop canopy to produce conidia and initiate infections (Romanazzi and Feliziani 2014).

B. *cinerea* has two infection pathways, one is related to conidia and the other one belongs to mycelium. Conidia infect inflorescences, young clusters, and ripening berries while mycelium is responsible for the berry-to-berry infection. Grape inflorescences are more susceptible at flowering (beginning, full, and end of flowering) than at earlier growth stages or at fruit swelling or berries groat-sized stages. On inflorescences and young grape clusters, infection severity increases with hours of wetness, and the optimal temperature for infection is about 20°C. Infection incidence in mature grape berries is higher at temperatures between 15 and 25°C than at other temperatures and increases with increasing hours of wetness or high relative humidity. Moreover, disease incidence is higher on wounded rather than on unwounded berries especially when wetness is short, or humidity is low (González-Domínguez et al. 2015).

B. cinerea can infect leaves in spring, where it grows at the margin of the blade, and flowers that are highly susceptible, particularly dehiscent floral parts. The disease development in grape berries depends on the genetic structure of the pathogen population in summer but is also related to key factors, including climatic conditions, cluster architecture, and berry susceptibility. Berry infection results mostly from conidia germination and penetration, favored by the presence of wounds at the surface of the fruit, in particular insect injuries, and spread by fungal vegetative filaments (mycelium) from one berry to the next (Bélanger et al. 2011).

The first observation of grey mould is in the foliage. Shoots and buds may turn brown and necrotic in early spring. The leaves might show large, reddish-brown patches. During periods of high humidity, grey mould can make leaf lesions. The fungi could affect yield at this stage by infecting the inflorescences and causing flower drops. However, the most common symptom is berry infection in late summer (Extension Service 2015).

Bunch rot often begins when blossoms become infected during rainfall. The pathogen invades the flower parts and becomes dormant until veraison. At veraison, individually infected berries in the cluster turn brown on white cultivars or reddish on red and black cultivars due to enzymes produced by the fungus and fungal invasion of the pulp. At this stage, fungal enzymes break down the epidermis and it easily slips off the berry. If temperatures are moderate, moisture is high, and wind speed is low, epidermal cracks will form in which fungal growth produces mycelium and spores resulting in the characteristic gray, velvety appearance of infected berries. The fungus can then spread from berry to berry causing a nested appearance of infected berries. If conditions remain favorable, the disease can result in a high percentage of berries being rotted and if the disease is severe enough to reach the rachis, the raising of infected berries can occur.

The fungus can penetrate grape berries through wounds; it can directly penetrate undamaged berries after veraison. The berry skin and epicuticular wax are the main protection from infection. Any chemicals or cultural practices that alter these physical and chemical defenses will change the susceptibility of the berry to infection.

In infected berries, cracks appear in the skin. The spores develop first in the cracks and then spread over the entire berry. The infection of other berries by the rapidly growing fungus and airborne spores contributes to the extremely rapid increase in disease observed after rains. Under optimal conditions, *Botrytis cinerea* can infect a berry, destroy it, and begin to produce spores in only 3 days. After infection, the berry may dry up if high temperatures and low relative humidity prevail (Broome J.C. 1995).

Figure 1.2. The first photo from left and above: Spring Botrytis infection on the leaf (Photo: L. J. Bettiga.), the second photo: A Botrytis-blighted flower cluster (Photo: W. J. Moller.), the third photo: Clusters of Botrytis spores on long stalks (conidiophores) on a berry surface (Photo: L. J. Bettiga.), the first photo from left and bottom: Raising caused late in the season from Botrytis infection on Riesling (Photo: L. J. Bettiga.), the second photo: Warm, dry weather at harvest can desiccate Botrytis-infected berries (Photo: L. J. Bettiga.) (Flaherty 1981).

B. cinerea is unable to directly infect the cuticle of the fruit but entered the sub-stomatal cavity where further growth ceases due to host defense responses. Close to ripening, conidial infections directly penetrate the fruit cuticle. In addition to stomatal infections, cuticular micro-cracks have been suggested as possible infection pathways, as in grapes. These cracks originate from microscopic fractures on the berry surface which rapidly enlarge as the berry swells after rainfall near harvest thereby facilitating infection (Philip A G Elmer and Michailides 2007). Grey mould losses in viticulture all around the world, reaching 20–50% of yield losses in grapes, due to rotting of ripe bunches in the post-harvest period. During contact with the plant, *B. cinerea* causes cell death by producing phytotoxins, cell wall degrading enzymes, and controls the host metabolism to facilitate colonization. The high relative humidity and moderate temperatures during the grapevine vegetative season favor the development of this fungal pathogen (Fedorina et al. 2022). *Botrytis cinerea* shows an extraordinary variability in phenotypic traits, because of this

fungal pathogen on mechanisms underlying its broad variation and adaptation capabilities such as mating system and sexual behavior and other sources of variation (chromosome number, mycoviruses, transposons, and vegetative compatibility). A *Botrytis cinerea* epidemic comprises a sequence of processes (perennation and infection, colonization, conidiation, and conidia dispersal), each of which is influenced by the host and the surrounding environmental conditions, such as temperature, rain, humidity, and wind. The other factors which are effective in the epidemic include cultural practices, such as fertilization and fungicide usage, and host factors such as tolerance and phenology (Elad 2016).

In addition, the presence of *B. cinerea* infected grapes consistently increased insect fecundity and attracted females to oviposit (Philip A G Elmer and Michailides 2007).

As Pinot Gris is tight-clustered, it is highly susceptible to bunch rot. *Botrytis cinerea* can be a major constraint to high wine production for this variety in regions with high humidity conditions (Ferree et al. 2003).

By monitoring environmental conditions, it is possible to determine the time of the epidemic of the disease. The thermal-temporal position of the epidemic of *B. cinerea* varied between seasons. The condition of low temperature and wetness during the bloom like high temperature and low precipitation after veraison can affect the thermal temporal for the late epidemic. The first effect might happen on the flowering and fruit set and cluster structure which is linked to the bunch rot (Daniel Molitor et al. 2016). In addition to climate and environmental conditions, the training system of grapes has a great effect on the severity of diseases such as downy mildew and bunch rot grape. In Southern Brazil, researchers found the training system indicated a significantly lower area under the incidence and severity of disease progress and intensity of downy mildew and grey mould (Bem et al. 2015).

1.4. Viticulture Management for grey mould

1.4.1. Cultural Method

1.4.1.1. Early Leaf Removal

One of the effective practices for controlling grey mould is the removal of the leaves early in the season between flowering and veraison. This practice could decrease the fruit set, control yield per vine, and decrease the cluster rot. Because of removing the leaves, the carbon allocation to cluster sinks is reduced. Therefore, it causes less flower fertility and fewer berries to make a looser cluster morphology. In addition, it increases the airflow around the clusters and reduces cluster rot in tight-clusters varieties. However, this method with manual operation is expensive and it needs the available labor. For this problem, the application of mechanical leaf removal could have better results in saving cost and time. Furthermore, the application of early leaf removal in pre-bloom time could effectively reduce cluster rot (Vanderweide et al. 2020). This cultural practice indicates a major option for pathogen control in organic viticulture where fungicides are not allowed.

The other strategy for leaf removal is using a plant growth regulator like gibberellic acid. The application of this hormone depends on the application time and dose, and the plant's developmental stage related to the weather conditions during application. With a proper dose of hormone, at the full flowering stage of the plant, the application could cause loss of the cluster and reduce the disease severity (D Molitor et al. 2011).

In one case study, the gibberellic acid application has been indicated to reduce berry number in several cultivars. Especially at flowering, it reduced bunch compactness (assessed as berry per cm, LDI) by 25% when compared to the control-treated, mainly associated with a reduction in berry number per bunch (Wegher et al. 2022).

The studies have reported some cluster elongation with a little amount of GA3 if it was applied 20 days before full bloom (Ferree et al. 2003).

The other plant growth regulator prohexadione-Ca reduces single-berry sizes and the number of berries per cluster, effectively reducing the disease (D Molitor et al. 2011).

1.4.1.2. Cultivation Of Intraspecific Varieties

One of the approaches to decrease the severity of grey mould loss is the cultivation of intraspecific varieties with less sensitivity for example Carminoir (Pinot Noir x Cabernet Sauvignon). The disadvantage of this approach is the application of botryticides for better cultural measures in many regions (Daniel Molitor et al. 2018).

1.4.2. Chemical method

Every year, European wine growers apply 70000 tons of pesticides which cost two billion euros, and most of them are fungicides because fungal diseases can provide crop losses of up to 70%. However, European countries aim to implement a more sustainable approach to using plant protection products (Latouche et al. 2015).

In the past, the strategies to control grey mould were mainly focused on applying fungicides, especially botryticides. The botryticides are applied in different growth stages (mid-bloom, before berries touch, beginning of veraison, 2–4 weeks after veraison). However, the efficacy of these fungicides depends on the annual meteorological conditions. The most effective mycelial growth inhibitor of *Botrytis cinerea* is Fenhexamid (Daniel Molitor et al. 2018). This method could not be applied to organic farms.

1.4.3. The technologies used for controlling pests and diseases

There are some methods for detecting and preventing the loss of pests and diseases. One of them is breeding which may make a resistant variety to pests and pathogens. This method could be complemented by genetic modification techniques (transgenesis, cisgenesis, and intragenesis), especially with recent technologies like Crispr Cas 9 that could precis the selection of desirable traits. Recent genetic studies of grapes have also allowed identifying gene systems of resistance or susceptibility to the most common pathogens like grey mould. A resistant grape cultivar to grey mould significantly increases resistant gene expression after inoculation with *B. cinerea* (Fedorina et al. 2022).

The second method is surveillance and early detection which could accelerate solving the problem and prevent losses. This detection can be implied with different kinds of technologies varying from video imaging to artificial intelligence and they are applied to detect problems early before the pathogens and pests spread and cause widespread

damage. Many of these systems are linked to smartphones allowing farmers and other experts to make better decisions in the early stage of the disease. In one case study, hyperspectral disease detection models have been implemented using original field data or manually annotated data for detecting the disease in grapes (Bendel, Kicherer, et al. 2020).

The third method is applying new control agents or biopesticides. This method could control specific pests and pathogens with biological agents. One strategy is the bioengineering of the rhizosphere, which indicates stimulating the spread of introduced or local populations of beneficial microorganisms, and the creation of synthetic microbial communities to improve plant growth, and disease resistance. It indicated that after inoculation of grapes with various potential biocontrol agents (*Pseudomonas oligandrum, Trichoderma spp., Streptomyces sp., Pseudomonas protegens*), the development of some pathogens was suppressed, and plant growth was stimulated to grow more. In addition, arbuscular mycorrhizas (AM) fungal inoculation enhanced the growth of grapevine. *Bacillus* strains are known as biological bacterial agents that produce antifungal substances to limit the symptoms of grey mould on the leaves and reduce the symptoms of the disease (Fedorina et al. 2022).

The fourth method could be precision agriculture, which makes the application of plant health products more accurate and precise and can reduce the number of chemical product applications. Precision agriculture applies data from multiple sources such as sensors and satellites to improve crop yields study by the spatial variation in crop yield and increase the cost-effectiveness of crop management strategies including fertilizer inputs, irrigation management, and pesticide application.

Chapter 2
Precision Viticulture

2.1. What is Precision viticulture?

Digital agriculture and Precision Agriculture (PA) have been identified as drivers for placing wine production in a sustainable, economically profitable, and environmentally friendly context (Fastellini and Schillaci 2020). Precision viticulture (PV) is one of the most effective developments in viticulture. It is based on technologies that combine a global navigation satellite system (GNSS), onsite or aerial measurements of local microclimatic conditions, details of vineyard water and nutrient status, with measurements of several vine physiological parameters with infield sensors, satellite, and airborne remote sensing. These data could be corrected and then interpreted thanks to GIS software. The result could help with grape uniformity, which greatly affects wine quality. PV can identify comparatively similar areas. Some examples of PV like pruning and bud selection may permit growers better options to offset some of the disruption being caused by climate change (Jackson 2016).

PV monitoring tools like unmanned aerial vehicles (UAVs), aircraft, satellites, and proximal sensors can be used together to fully interpret the monitored fields.

The result is an operational map that can be loaded into variable-rate machines (VRT) to optimize field operations like fertilization, defoliation, irroration, phytosanitary treatments, and harvesting. In addition, a decision support system (DSS) allows agronomists to make better decisions at the right time and place. DSS for agriculture are the systems that provide information resources to contribute to farmers' decision-making, by integrating various forms of information required for growing crops (Kanatas et al. 2020).

There are some difficulties with the application of PV techniques. The most important one is the costs of these technologies. The others are unclear savings costs and the lack of knowledge of the technicians for using these technologies (Ammoniaci et al. 2021).

An example of the application of PV is using early yield prediction which is an important parameter in gaining the best grape production and quality. Ground observation and manual weighing are time-consuming and frequently provide low-resolution data. By applying high-resolution RGB images, a representative zone of vigor variability of the whole vineyard acquire. To estimate the production, an unsupervised recognition algorithm is applied to derive the number of clusters and size. There are two advantages to using these methods accuracy and timesaving (S.F. Di Gennaro 2019).

In one case study in the Chianti Classico DOCG area in Italy, with proximal sensing, a ground monitoring system equipped with two types of sensors to define vineyard features such as the plant vegetative vigor indexes (NDVI vigor index) and the canopy volumetry. By applying these tools, the knowledge of grapes improved, and the quality of the wine was achievable by selective harvest and through the pesticide calibration on the canopy (Sarri et al. 2015).

2.2. Precision Viticulture for early detection of disease

There are two branches to detect disease in the plant. The first class is invasive techniques involving destructive leaf sampling followed by chemical treatments after identifying the pathogen. The second one is non-invasive techniques to identify the impact of the pathogen on the physiological plant response. Most of them included sensors that measure temperature, reflectance, image analysis, or fluorescence and volatile organic compounds profiling-based technique for recognizing plant diseases (Sankaran et al. 2010).

2.2.1. Weather conditions and early detection

Weather conditions frequently are one of the main factors that can make desirable conditions for diseases in crops such as rain or high humidity, which can provide the favor situation to increase the risk of fungal diseases. For predicting the problem, meteorological monitoring is vital to have some indication of a possible infection. There

are some devices for making the warning. Devices (weather stations) that can predict the weather condition in real-time are needed to know precisely when an infection occurs.

In the last few years, new devices from the Internet of Things (IoT) have been used to obtain real-time in situ observations (mainly meteorological). The nodes of IoT contain low-cost sensors to monitor meteorological phenomena such as temperature, air/soil humidity, wind speed, wind direction, and rainfall. There are some models to warn the fungal diseases like *Botrytis cinerea* that are related to the data coming from the IoT nodes in real-time and can make an alert. Compared to the traditional method, the chemical product would be applied during the most effective time window against grey mould infections. It could make economic savings and reduce the possible impact on the environment (Oliver et al. 2019).

2.2.2. Application of Remote-Sensing for early detection

Remote sensing (RS) is a technique widely used for crop monitoring in precision viticulture systems and applied for the evaluation of canopy health and vigor status. Airborne and satellite imagery acquired during growing seasons can be used not only for early detection and within-season management of some crop diseases but also for the control of recurring diseases in future seasons (Yang 2020).

With both passive and active radiation, the RS systems permit data acquisition ranging from gamma rays to microwaves. Different RS systems are applied in capturing the infection symptoms such as scabs and pustules, physiological responses like changes in pigment content and water content, and structural changes such as canopy structure and landscape structure (J. Zhang et al. 2019).

2.2.3. Application of machine learning for early detection

Machine learning (ML) is an application of Artificial intelligence (AI) aiming to create an autonomous system for learning and predicting features. In the agriculture landscape, ML is useful to predict crop features from environmental data and crops' status. Machine learning is a method for predicting the disease of grapes in the early stage of the disease to decrease the losses to the wine producer. This method collects the two types of images to make a dataset to identify healthy and unhealthy plants. Image processing computer

vision and machine learning methods have been used to prevent the spread of disease and minimize the loss (Alessandrini et al. 2021).

2.2.4. Application of Proximal-Sensing for early detection

Proximal-sensing is based on the applying of ground-based moving vehicles carrying various types of sensors that are suitable for continuous measurements of soil or canopy parameters. The advantages of proximal are their high-resolution imagery, their total independence from external parameters and limitations, their suitability for small fields, and their simple application (Anastasiou et al. 2018). In one case study, two kinds of sensors were used sensors to catch the data such as GreenSeeker RT100 sensors calculating NDVI and Red/NIR indices in real-time, and ultrasonic sensors to estimate canopy thickness. These data evaluate the monitoring system performance regarding disease appearance, diffusion, and vegetative development variations due to the normal growing process of vines (Mazzetto et al. 2010).

2.2.5. Application of thermal imaging

When a stressed plant responds to the pathogen or water stress, it usually reveals by leaf temperature before visible symptoms appear. This temperature change could be evaluated by Infrared thermography (IRT) and indicated differences within individual leaves, plants, and crops showed the presence of disease in plants. Compared to optical, multispectral, and hyperspectral sensors, thermal sensors have been highlighted to be more effective at disease-induced early modifications. One case study sought to detect downy mildew on the grapevine leaves at the early stages of development using thermal imaging technology (Cohen et al. 2022).

2.3. Grape-related technologies

2.3.1. Scouting

Scouting is one of the most important methods for monitoring pests and diseases. Scouting means a human supervising the crops. Regular scouting has been used for the early detection of disease before it starts to grow in a vineyard. With regular scouting and

analyzing the weather condition, the farmers could decide the best time to apply the pesticides. The scouting frequently starts when shoots are 3 – 5 and continues until shoots are at least 12. For scouting, it is important to consider areas that are susceptible to infestations such as border rows near woods, overgrown areas, tree lines, or any protected areas around the vineyard where leaf debris might collect. Early scouting in the season, especially in highly susceptible varieties or newly planted vineyards is frequently recommended (Bryan Hed 2016).

Some new methods of the automatic collection of field data have been promoted to use in precision agriculture. Autonomous field scouting robots have recently been applied for some pest control. In this method, vision sensors and ranging sensors have been used to quantify crop statuses such as vigor, diseases, nitrogen stress, and other stresses.

In one case study, the scouting robots applied artificial lighting. Proximal sensing can acquire crop information with a higher ground resolution and can extract crop shape information more accurately than aerial sensing. In addition to applying daytime sensing, nighttime sensing was used as a unique method. The research was to evaluate the accuracy of the shape information and spectral information of soybeans obtained by estimating the FVC (The fractional vegetation cover) and SPAD (The soil plant analysis development) values and to devise a highly accurate crop growth sensing method using agricultural robots and it was estimated by NDVI. This method can minimize the need for human intervention during crop sensing (Yamasaki et al. 2022).

In addition to robots, there are all terrains vehicles equipped with many sensors. The other methods include spectroscopy, multispectral and hyperspectral imaging, chlorophyll fluorescence, thermography, electrical resistivity, laser imaging detection and ranging, and computer vision and the platforms where they are generally mounted or embedded for either proximal or remote monitoring (Tardaguila et al. 2021).

2.3.2. NIRS

Near-infrared spectroscopy is an analysis method of choice in food and agriculture with minimal sample preparation. In the wine industry, the most used NIR method is for the analysis of wine ethanol. The use of NIR for detecting fungal contamination has been implemented for different kinds of diseases such as grey mould and powdery mildew in

grapes. This method can apply for rapid assessment of contamination; however, it requires a reference analysis for calibration and validation such as DNA analysis which could not be a quick and cheap test as quantitative PCR. This method was used to predict the powdery mildew of grapes. The grapes with different degrees of powdery mildew were collected then samples were homogenized and analyzed for powdery mildew DNA content, and scanned by reflectance spectroscopy, over a wavelength range covering the visible and near-infrared (NIR) regions of the electromagnetic spectrum. The results indicated the correlation between the powdery mildew DNA content, and spectral information generally with the visual infection classification (Stummer Belinda et al. 2007).

In one study case, to assess grape infection rapidly, the vis/NIR spectroscopy in a view of a grape classification directly at the checkpoint station entering the winery was applied.

For this research, the white and red wine varieties bunches were used that were naturally infected with major grape diseases such as *Botrytis cinerea*, powdery mildew, and sour rot. The analyses were applied to grape to test the performance of vis/NIR devices to classify healthy and infected samples. The results demonstrated that optical devices are capable to provide useful information for better management of the vinification process (Tugnolo et al. 2017).

An example of near-infrared application in the field is the detection of leaf-miner infestation on tomato leaves by an optical measurement system with Fourier transform near-infrared (FT-NIR) systems. The infested tomato leaves had lower reflectance values than the healthy leaves due to the disrupted leaf structure caused by leaf miners with increasing severity of the damage, the leaf reflectance increased while the leaf water content decreased (Xu et al. 2007).

In one case study for Grapevine yellows (GY), a serious phytoplasma-caused disease detection in vineyards, greenhouse plants were analyzed by hyperspectral imaging and disease detection models (Radial-Basis Function Network). The identification of infected greenhouse plants was successful reaching up to 96% (Bendel, Backhaus, et al. 2020).

Visible and near-infrared (VIS-SWIR) spectral systems can determine damages caused by plant diseases and pests by reflectance. This method is stable and offers reliable monitoring results. However, it performs weakly on early detection (J. Zhang et al. 2019).

2.3.3. Fluorescence

Fluorescence monitoring is a method used in different aspects of research such as agronomy, forestry, marine environment, ecotoxicology, plant physiology, and plant breeding. In this method, Chlorophyll a (Chla) fluorescence can be indicated photosynthetic efficiency and provides information on the relationship between the structure and function of photosystem II (PSII) reaction center (RC) and core complexes.

The so-called JIP-test is a means to analyze the polyphasic rise of the Chl a fluorescence transient and it develops to find in vivo the “vitality” of plants and the adaptive behavior of the photosynthetic apparatus to different stresses. This method was used for the analysis of plants without visible disease foliar symptoms (Esca disease) that were compared with those showing symptoms. This is an important wood disease that impedes plant water transport by clogging the xylem vessels. The pathogens grow slowly into the vascular tissues and aerial symptoms are visible after several years. This type of effect is not detectable for years, due to the long latency time of the disease. The advantage of application fluorescence is the alteration of the photosynthetic apparatus could be detected 2 months before the appearance of foliar symptoms in autumn (Christen et al. 2007).

For downy and powdery mildew diseases in grapes, after two weeks of infection, the plant starts to produce a phytoalexin which produces a UV-induced violet-blue fluorescence (VBF). This autofluorescent property of the stilbenoid phytoalexins, which is found in infected leaves, is used to detect the presence of diseases. Fluorescence sensor based on LED excitation and filtered-photodiode detection that is designed to work in the field under daylight conditions. Early detection of the disease in the field is to achieve the aim of precision agriculture (Latouche et al. 2015).

For grey mould disease, 48h after inoculation, at the periphery of the lesion on leaves, but not inside the colonized tissue including dead cells the blue fluorescence could be detected. The autofluorescence response of mature grape berries to *B. cinerea* infection is used to achieve early detection. Using image analysis and edge detection over UV-epidermal transmittance measured at 690nm, it was possible to detect botrytized berries as early as 3 DAI (Bélanger et al. 2011).

2.3.4. Colored images analysis/processing/ color space analysis

Machine learning (ML) algorithms or deep learning (DL) algorithms are so useful for early disease detection. A deep convolutional neural network (DCNN) algorithm could identify and classify grape diseases based on multi-band leaf images. Multi-band images are composed of visible light wavelengths such as Red, Green, and Blue (RGB) bands. The proposed approach uses an image dataset of grape crops. This developed model can provide accuracy close to or even more significant than the accuracy obtained for some pre-trained models using transfer learning. It was reported one model achieved an accuracy of 99.34% and equal values for precision. It showed the models' capability to accurately identify and classify grapes' common diseases based on the RGB leaf images (Math and Dharwadkar 2022).

There are several steps in preparing the images for disease detection including image acquisition, image pre-processing, image segmentation, feature extraction, and classification. The images captured by a camera are in RGB (Red, Green, and Blue) form, and a device-independent color space transformation is applied for the color transformation structure.

For the preprocessing step, the images are clipped and cropped to get the interesting part of the images and remove disturbing elements. Then the filter is applied to smooth the images and image enhancement is carried out for increasing the contrast. The RGB images are converted into gray images. Because color images have primary colors red, green, and blue, it is difficult to implement the applications using RGB as their range from 0 to 255. The segmentation can be done using various methods like otsu's method, and k-means clustering. K-means clustering is used for the classification of objects based on a set of features into K number of classes. The classification of the object is done by minimizing the sum of the squares of the distance between the object and the corresponding cluster. Feature Extraction is important for the identification of an object. In many applications of image processing, feature extraction is used. Color, texture, morphology, and edges are the features that can be used in plant disease detection. In some cases, color, texture, and morphology are used as a feature for disease detection. It was found that morphological results could give a better result than the other features. Texture means how the color is distributed in the image, the roughness, and the hardness

of the image. It could be used for the detection of infected plant areas. After feature extraction, the learning database images are classified by using a neural network. These feature vectors are considered neurons in ANN (Khirade and Patil 2015).

2.4. Compactness

2.4.1. Compactness of berries and its effects

One of the most important traits of grapevine is bunch compactness or bunch density which could affect the commercial quality of the wine. Bunch compactness refers to the way that how berries are arranged in the bunch and to the rate of free space between them. Bunch compactness relates to the morphological volume of the bunch to its solid component. The solid component is determined by the number of berries and their individual size. These two major growth stages (berry formation and berry ripening) largely define the final berry size. With compact bunches, grapes are more susceptible to diverse pests and diseases like bunch rot. Compactness in bunches could cause berry cracking and the leakage of juice, making free water and nutrients for fungal spores' germination and mold growth. The dense berries restrict airflow between berries and could increase the internal temperature and humidity in the bunch. In addition, it causes the berries expose to the UV radiation of the sun and the berries start to generate more wax on the skin and make the thicker skin which could increase the production of phytoalexin against pathogens and reduce the effect of fungicide in the inner side of berries. The compactness also affects the quality of wine and reduces the crop yield which causes more economic losses. Bunch rot also reduces the quality of wines by generating off-flavors, oxidative damage, premature aging, and difficulties in clarification during the winemaking process.

Berries with high compactness ripe more heterogeneously because the inner berries receive little direct solar radiation. There could be a relationship between solar radiation and relevant parameters for winemaking, including juice pH, sugar, and organic acid variation, amino acids, anthocyanin and flavonoids accumulation, and the synthesis of tannins, stilbenes, terpenes, carotenoids, and methoxypyrazines (J. Tello and Ibáñez 2018).

2.4.2. Compactness and the evaluated methods

There are several methods for evaluating the compactness of berries. Bunch compactness is basically analyzed by visual and qualitative methods that classify grapevine bunches according to their general appearance. The most used method to evaluate this trait is the Organisation Internationale de la Vigne et du Vin (OIV) descriptor code 204 for bunch density. This descriptor classifies bunches into five categories by considering the mobility of the berries and the visibility of the pedicels: very loose (1); loose (3); medium (5); compact (7) and very compact (9). This method is simple, cost-saving, rapid, and nondestructive tools. On the other hand, it needs trained evaluators and an objective and continuous variable (J. Tello and Ibáñez 2018). However, there is a problem with this method when several evaluators are responsible for rating clusters, then differences between each can be an additional source of error. The other issue is that no population diversity can recognize if clusters have similarly compact, resulting in similar or identical OIV 204 scores (Underhill et al. 2020).

For the indirect method the fact that compact bunches are less flexible than loose ones, has been used for the qualification of the trait. For example, the bending index was applied to the categories. Another method was inter-berry spacing, with loose bunches having more space between berries than compact ones.

Other indirect measurements aim to determine how much space in the morphological volume is not actually filled by berries. The actual volume of the bunch of solid elements may be easily measured by the immersion of the bunch in a bucket filled with water and determining the amount of water displaced, following Archimedes ‘principle. However, the determination of the morphological volume is more complex, especially in loose bunches, because any modification in the natural arrangement of the berries will modify it.

Recently, methods based on the analysis of two-dimensional (2D) and three-dimensional (3D) images have been applied for the automated reconstruction of grape bunch architecture which could be a more precise and objective measurement of bunch morphological volume (J. Tello and Ibáñez 2018).

For objective methods, there are some bunch compactness indexes for example the index for the number of berries or bunch mass divided by the bunch length which is the

most typical objective estimator for the evaluation of bunch compactness. The other index is calculated by dividing either the number of berries per bunch or the bunch mass by the sum of the length of the rachis and of its first branch. These kinds of indexes are simple, however, their use in some cases may be uncertain because different bunch morphologies can be found in some species.

Some novel methods based on phenotyping tools like analyzing bunch images of the F1 population (the first filial generation plants offspring resulting from a cross-mating of distinctly different parental types) and determining a new compactness ratio calculated from the difference between the area of the bounding box (bunch length × bunch width) and the visible area of the bunch or estimated through the automatic analysis of RGB images of bunches (J. Tello and Ibáñez 2018).

In one research, several indexes were applied to find the effective indexes to define the compactness of grapes. Two of them are based on the combination of six metrics from bunches (bunch weight, number of berries per bunch, number of seeds per berry, bunch length, first ramification length, and either pedicel length or number of ramifications per bunch, respectively). These two indexes are more suitable for inter-varietal studies where obtaining quantitative data is critical. Another selected index is based on two easy-to-measure characteristics of the bunch (weight and length), and it is proposed as a fast estimator (J Tello and Ibáñez 2014).

In one study, images of different red grape cultivars were taken with a color camera, and their bunch compactness was determined by visual inspection. A predictive partial least squares (PLS) model was developed to estimate bunch compactness from the morphological features extracted by automated image analysis. The PLS model indicated a capability of 85.3% for correctly predicting the rating of bunch compactness from different grapevine varieties. The most discriminant variables of the model were highly correlated with the tightness of the berries in the bunch (proportion of visibility of berries, rachis, and holes) and with the shape of the bunch (roundness, compactness shape factor, and aspect ratio) (Cubero et al. 2015).

2.4.3. Compactness and 3D methods

The novel methods based on computer vision are used for Automated cluster compactness estimation in commercial vineyards. With a mobile sensing platform, image acquisition allows the user to take images in extensive vineyards, which could be automatically geo-referenced. This method could help to make a map showing cluster compactness. Also, it can help to indicate the zones with similar values for cluster compactness, which is important for sorting grapes before harvest. This non-invasive nature of the system could also enable early identification of very compact clusters to establish strategies against fungal diseases which could help to drive decisions on harvest classification or differential fungicide spraying. These kinds of methods could estimate wine grape cluster compactness using RGB computer vision on-the-go with machine learning technology under field conditions. It is so time-saving method to improve decision-making in precision viticulture and the wine industry (Palacios et al. 2019).

In recent past years, few studies have been done, applying two- or three-dimensional (2D or 3D) sensor systems. Automatic and semi-automatic image analysis was often used to extract phenotypic traits from Red-Green-Blue (RGB)-images of grapes. Compared to 2D imaging, 3D data are fully informative and more precise. An additional dimension gives more important information about the shape, structure, and volume of the scanned object.

It is required to apply the 3D data under controlled lab conditions to obtain the full 360° structure of the bunch (Rist et al. 2019).

One method that is applied in research is multi-perspective imaging analysis combined with multivariate modeling to predict grape bunch compactness. This multivariate data analysis is including partial least squares, multiple linear regression, and principal component regression. The partial least squares model was the best performed, predicting bunch compactness with a high correlation coefficient of prediction.

In this study, after harvesting and collecting the bunches of grapes, bunch wings were removed, and the main part of the bunch was applied to estimate the compactness. The grapes were imaged with two mirrors to make three perspectives. The compactness of bunches was scored by technicians based on the method outlined in OIV. The density of grapes was calculated. The descriptors such as the area and perimeter of the bunch were

measured, and the height and width were calculated by a small enclosing rectangle method. The bulk density of the grape bunch was linearly related to compactness. The morphological features of grape bunches and their derivative variables were digitized using image processing descriptors and were regressed with the measured compactness. The performance of the multi-perspective imaging method could be applied to automate the postharvest assessment of the compactness of grape bunches (Chen et al. 2018).

Chapter 3
Experimental Tests

3.1. Introduction

3.1.1. The importance of non-contact grape characterization

Today winegrowers face a lot of issues related to climate change such as changing weather patterns, compressed season, drought, and heat wave. On the other hand, they face to lack of labor and higher production costs. Therefore, it is needed to apply means to monitor the biophysical characteristics of grapes and analysis the management practices in the vineyards such as irrigation, nutrition, yield analysis, and prediction the diseases (Tardaguila et al. 2021).

For example for yield analysis, each field in agriculture is not considered to be uniform, as generally done in conventional agriculture, it needs to manage with site-specific management to increase the efficiency of inputs in the fields (Santesteban 2019). In a vineyard with a fixed planting distance, the sampling points can be applied to individual vines which are geo-referenceable, and, if data collection is carried out year after year, historical series of important value for crop management can be obtained to carry out some type of differential action (site-specific management) (Arnó et al. 2009).

Research interest shows an increasing proportion of research work in precision agriculture belonged to precision viticulture and this makes a high impact on increasing the quality of grapes and changes in the wine price (Santesteban 2019).

An important group of technologies is those associated with remote means far from the ground and proximal named for close-to-the-ground sensing which acquires information about on-ground targets such as plants and soil. It is important to use a tool to obtain detailed data and information about the product that makes the best decision with environmentally and financially sustainable practices. Precision Viticulture tries to apply the technology to this sector. Some non-invasive sensing technologies such as LiDAR, spectroscopy, and thermography can be applied to portable sensors or mounted with varied platforms. For detecting diseases and pests in vineyards hyperspectral

imaging, multispectral imaging, computer vision, spectroscopy, and thermography are often used (Tardaguila et al. 2021).

For cluster compactness assessment, computer vision methods try to find the best way. Some methods are working under controlled laboratory conditions, which require the destructive collection of clusters in the vineyard. It is needed to apply a method for large-scale real-time disease monitoring under field conditions. It is important that the plant disease detection tool should be rapid, specific to a particular disease, and sensitive for detection at the early onset of the symptoms. This method also is reliable for diagnosing diseases and must be overcome when analyzing the great number of samples required. The process of computer vision includes accusing, processing, analyzing, and extracting the data of images to provide numerical information such as estimating and predicting the features of the target objects. It can be a reproducible and accurate tool to assess defect detection, color estimation, and shape and size analysis. In addition, with the application of artificial intelligence, it could be more precise (Tardaguila et al. 2021).

3.1.2. OIV grape characterization protocols

Morphological characteristics descriptions have a key role in the studies related to grapes. Because for research studies the researcher had to define the characteristics based on the research aims these definitions are varied. On the other hand, there were no uniform lists of distinctive characteristics. Therefore, OIV (International Office of the Vine and Wine), UPOV (International Union for the Protection of New Varieties of Plants), and Bioversity (formerly known as IPGRI, International Plant Genetic Resources Institute) decided to arrange the descriptive characteristics which they were using up to now for differing ends. The definition of these distinctive characteristics is done by the OIV's Group of Experts. The index cards describe characteristics and make up a reference code common to OIV, UPOV, and Bioversity. The table of characteristics comprises not only characteristics distinguishing the grape varieties but also characteristics that indicate the agronomic aptitudes of grape varieties.

Each characteristic is provided with an OIV number with words that correspond to a certain figure note. These notes are the smallest units for describing a characteristic. A scale from 1 to 9 is defined.

Qualitative characteristics should be those which show discrete discontinuous states with no arbitrary limit on the number of states. Quantitative characteristics are those that are measurable on a one-dimensional scale and show continuous variation from one extreme to the other. They are divided into notes from 1 to 9. Notes 1 to 3 represent a weak expression, while notes 7 to 9 are strong or very strong. Which parts of the scale of words or notes are chosen for the definition of the single states, depends on the extent of variation within the single characteristic and the possibility of their subdivision.

Characteristics are recognized by visualization, measuring or weighting, DNA or isoenzyme analysis, or sensory observation (taste, smell). Further details are listed within the single characteristics. For example, statistical methods must be considered when observations are made over the years. The resistance of grape varieties to fungus diseases is to be observed under field trials over several years without the use of chemical plant protection. Notes 1 to 3 represent susceptibility, whereas notes 7 to 9 represent notes for resistance. These defining characteristics included different characteristics of the young shoot, shoot, woody shoot, young leaf, mature leaf, flower, Inflorescence, berry, bunch, yield, sugar content, rootstock, and cluster.

In this study, some descriptive characteristics are considered related to fruit description to analyze the compactness of bunches. In table 3.1 these characteristics are introduced (Vin 2009).

Table 3.1 The list of the applied characteristics of grape shape from the (OIV) table.

Characteristic	***Codes N°***	***Notes***	***Definitions***
Bunch: length (peduncle excluded)	OIV 202	Very short to very long (80 mm to over 240 mm) (1-9)	Observation at maturity. Mean value of the largest bunches of 10 shoots. To be measured: distance from the uppermost to the lowest berry of the primary bunch.
Bunch: width	OIV 203	Very narrow to very wide (40 mm to over 200 mm) (1-9)	Observation at maturity. Mean value of the largest bunches of 10 shoots. To be measured: maximum distance between the lateral berries of the primary bunch.
Bunch: density	OIV 204	Very loose to very dense (1-9)	Observation at maturity. Examination of the largest bunches of 10 shoots. 1 = berries clearly separated, many visible pedicels; 3 = berries in loose contact with each other with some visible pedicels; 5 = densely distributed berries, pedicels not visible, berries are movable; 7 = berries not readily movable; 9 = berries deformed by compression.
Bunch: length of peduncle of the primary bunch	OIV 206	Very short to very long (30 mm to 110 mm) (1-9)	Observation at maturity. Mean value of the largest bunches of 10 shoots. To be measured: distance from insertion point on the shoot to the 1st ramification of the primary bunch. There is a knot-like thickening on the bunch peduncle, from which a secondary bunch or a tendril may arise.
Bunch: lignification of peduncle	OIV 207	at the base only to more than the middle (1-7)	Observation at maturity. Examination of all bunches of 10 shoots. Lignification of peduncle = brown coloring of the peduncle. Remark: variable, dependent on conditions of maturity
Bunch: shape	OIV 208	cylindrical (1) conical (2) funnel-shaped (3)	Observation at maturity. Examination of the largest bunches of 10 shoots. Description of the bunch shape between 3/5 and 4/5 of the axis. Wings in the upper part and the tip are excluded from observation.
Bunch: number of wings of the primary bunch	OIV 209	Absent to more than 6 wings (1-9)	Observation at maturity. Examination of the largest bunches of 10 shoots. Remarks: wings = lateral branches on the main axis of the primary bunch, which are clearly longer than the other branches.
Berry: length	OIV 220	Very short (8 mm) to very long (more than 28 mm) (1-9)	Observation at maturity. The mean value of 30 nondeformed and normally sized berries was taken from the middle part of 10 bunches (measuring unit: mm without decimals).
Berry: width	OIV 221	Very narrow (8 mm) to very wide (more than 28 mm) (1-9)	Observation at maturity. The mean value of 30 nondeformed and normally sized berries was taken from the middle part of 10 bunches (measuring unit: mm without decimals).
Berry: uniformity of size	OIV 222	Not uniform (1) Uniform (2)	Observation at maturity. Examination of 10 bunches. Remark: variable, also dependent upon seed set (number of seeds/berry).

Berry: shape	OIV 223	obolid (1) globose (2) broad ellipsoid (3) narrow ellipsoid (4) cylindric (5) obtuse ovoid (6) ovoid (7) obovoid (8) horn-shaped (9) finger-shaped (10)	Observation at maturity. Examination of 30 berries not deformed by compression taken from the middle part of 10 bunches.
Berry: uniformity of skin color	OIV 226	Not uniform (1) Uniform (2)	Observation at maturity. Examination of 3 0 berries taken from the middle part of 10 bunches.
Berry: hilum	OIV 229	little visible (1) visible (2)	Observation at maturity. Examination of 30 berries taken from the middle part of 10 bunches.

3.1.3. Review of previous methods

The subjective evaluation method of grape compactness is, assessing the visual shape of grapes by the descriptor code 204 for bunch density defined by the Organisation Internationale de la Vigne et du Vin (OIV). The scores are defined from 1 to 9 with five categories. The other method is applying the density index based on the stem bending and there are varied categories and defined scores for it.

Inter-berry spacing is another one that uses the distance between two randomly chosen berries by inserting wedges in the inter-berry space. The other close method to inter-berries spacing is to determine how much space in the morphological volume is not filled by berries. It could be done by immersion the bunch in a bucket filled with water or using the melted paraffin. Estimating the morphological volume of the bunch assimilates it to a perfect cone where length is the maximum bunch length, and radius is half of the widest bench width. However, this method only does not consider irregularities and it is not applicable to other shapes of grapes such as cylindrical. Object methods based on a bunch of quantitative variables. The most important estimate index for the compactness of a grape is the number of berries divided by the bunch length or berry number by bunch

mass. After some modifications to the indexes, alternative compactness indexes were presented. They are based on the combination of six bunch metrics, indicating many factors involved in determining bunch compactness. They are useful to quantify differences between different cultivars and between clones of a single cultivar (J. Tello and Ibáñez 2018).

Table 3.2. Indexes of compactness estimation (modified table from (Tello and Ibáñez 2014))

Indexes	*Equations*	*References*
1	BW (g) / [RL (cm) + 1RL (cm)]	(Fermaud Villenave d'Orono France.) 1998)
2	BB / [RL (cm) + 1RL (cm)]	(Valdés-Gómez et al. 2008)
3	BB/BL (cm)	(Pommer et al. 1996)
4	[ABV (mL)/MBV (mL)] × 100	(Sbpahi 1980)
5	ABV (mL) / (RL (cm) + 1RL (cm) + 2RL (cm))	(Sbpahi 1980)
6	BW (g) / (RL (cm) + 1RL (cm) + 2RL (cm))	(Sbpahi 1980)
7	ABV (mL) × RB / (RL (cm) + 1RL (cm) + 2RL (cm))	(Sbpahi 1980)
8	BW (g) × RB / (RL (cm) + 1RL (cm) + 2RL (cm))	(Sbpahi 1980)
9	[CBV (mL) - ABV (mL)] × 100 / ABV mL	(Shavrukov et al. 2004)
10	BW (g) / BL (cm)	(Sternad Lemut et al. 2010)
11	BW (g) / MBV (mL)	(Ferreira and Marais 1987)
12	BW (g) / [BL (cm)]^2	(J Tello and Ibáñez 2014)
13	ABV (mL) / [BL (cm)]^2	(J Tello and Ibáñez 2014)
14	BB / (BL (cm) + 1RL (cm) + 2RL (cm))	(J Tello and Ibáñez 2014)
15	BB / ∑ IL (cm)	(J Tello and Ibáñez 2014)
16	10.368 + [0.015 x BW (g)] + (0.002 × BB) [-0.443 × BL (cm)] + (0.018 × 1RL)	(J Tello and Ibáñez 2014)
17	BW (g) × BB / ([BL (cm)]2 + 1RL (cm))	(J Tello and Ibáñez 2014)
18	BW (g) × BB × (1 + SB) / ([BL (cm)]2 × 1RL (cm) × PL (mm))	(J Tello and Ibáñez 2014)
19	BW (g) × BB × (1 + SB) / ([BL (cm)]2 × 1RL (cm) × RB)	(J Tello and Ibáñez 2014)

1RL: First ramification length; **2RL**: Second ramification length; **ABV**: Actual bunch volume; **BL**: Bunch length; **BW**: Bunch weight; **CBV**: Conical bunch volume; **IL**: Internode length; **MBV**: Morphological bunch volume; **BB**: Berries per bunch; **RB**: Ramifications per bunch; **PL**: Pedicel length; **RL**: Rachis length; **SB**: Seeds per berry.

In table 3.2., the indexes of the compactness of grapes that were applied in various studies are summarized.

The other equation for calculating compactness is defined as the ratio of the area of an object to the area of a circle with the same perimeter.

Compactness = 4π. area/perimeter ^{2}

Objects with an elliptical shape, or irregular boundary rather than smooth, will decrease the measure.

Compactness = perimeter ^{2} /4π. area (Wirth 2004).

The recent methods, applying automatic analysis of RGB images with the determination of relevant bunches of compactness-related variables, such as the proportion of pixels in the image corresponding to berries, rachis, and holes, and a series of calculated variables related to the shape of the bunch, such as roundness, compactness shape factor and aspect ratio, a mathematical model presented the prediction of compactness.

The methods with evaluated 2D image analysis and 3D scanning technologies used two factors visibility of rachis and holes and the compaction of the berries. The novel image-based technologies use different variables related to bunch architecture and highly related to visual bunch compactness such as the area of the bunch image covered by the berries, holes, and rachis and the concavity of the bunch and the intersection between berries (J. Tello and Ibáñez 2018).

In recent studies, the morphological features used to characterize the shape of an object include the length of the major and minor axes, area (A), perimeter (P), the ratio between area and perimeter (AP), length (L), maximum width (MW), aspect ratio(AS), compactness shape factor (CSF) and roundness (RD) of the bunch, as well as the width at 25% (W25), 50% (W50), and75% (W75) of the length of the main axis, and proportion of the area corresponding to berries (AB), rachis (AR), and holes (AH) in the bunch (Cubero et al. 2015).

3.1.4. Measuring the compactness for 2D (two dimensional) shape

Compactness is one of the most important properties of a shape. The common way to calculate the compactness of an object is to measure the ratio of (perimeter^2)/area which is dimensionless and minimized by a disk and depends in large part on the perimeter in the 2D domain. In fact, objects have noisy perimeters or enclosing surfaces, that can affect the measuring of compactness. In another study, the method presented alternative area-perimeter ratios for the measurement of the 2D shape compactness of objects, and it is important to evaluate the effect of external disturbance on natural objects (Bribiesca

2008). Some methods proposed can be grouped into four categories: area-perimeter measurement, reference shape, geometric pixel properties, and dispersion of elements of the area (Li et al. 2013).

The suggested measurement in one study can be used to calculate compactness for connected and disconnected objects and is invariant under translation, rotation, and scaling. The method is so simple by means of the use of one equation and it varies continuously from 0 to 1. To measure compactness, the measures of discrete compactness of different objects are calculated. The measure of discrete compactness for 2D shapes composed of pixels is obtained and defined (Bribiesca 2008).

Three criteria are defined to evaluate the efficiency and effectiveness of compactness measures. The first is robust, which means the ability to measure the compactness of any shape and be insensitive to uncertainty. In addition, it must be stable for a given fixed shape related to changes in size and spatial resolution. The second one is computationally efficient. And the third one is additive which means easy to compute, reduces computational complexity, and improves computational efficiency and effectiveness when used in real-world applications (Li et al. 2013).

3.1.5. New proposed 3D approach and parameters extractions

In some studies, the 3D methods analyze the bunch compactness based on the scanners or sensors by using a laser. In one study the 3D Scanner was applied to provide not only bunch architecture traits but also individual berry characterization by combining 3D modeling and machine learning algorithms (Herrero-huerta et al. 2022).

Grape bunch architecture is related to the compactness of the bunch and is mainly influenced by the berry number, berry size, total berry volume, and bunch width and length. For assessing the bunch architecture, the 3D imaging method can be applied (Rist et al. 2019).

In the 3D approaches, the compactness of an object depends on the enclosing surface area with the volume and can be defined by the ratio(area3)/(volume2), which is dimensionless and minimized by a sphere and is usually described on the enclosing surface area in 3D. One recent method applied the measure of discrete compactness of 3D shapes composed of voxels, related to the sum of the contact surface areas of the

face-connected voxels for 3D shapes. Volumetric representations are used for rigid solids by means of spatial occupancy arrays. Therefore, the solids are represented as 3D arrays of voxels which are marked as filled with matter. Some studies suggested applying discrete compactness which is in tight correspondence to those invasion features (Bribiesca 2008).

The other method for reconstructing 3D models from processed images is Photogrammetry. It has high efficiency and the radiometric and geometric characteristics of objects with great accuracy. This method with computer vision tried to estimate the yield parameters in the productivity of a vineyard such as the volume, the mass, and the number of berries per bunch (Herrero-Huerta et al. 2015).

3.2. Experimental plan

In this study, photogrammetry techniques were used to build 3D models of several Pinot Gris and Pinot Noir clones. A large number of measures and indexes were extracted from the collected values of the 3D shape grapes. The relation between output data and the grape's shape characteristics was analysed. To find which descriptors have a high correlation to grey mould severity, a multiple linear regression model was created. Two models were presented, divided into 2D and 3D descriptors. Two factors were compared for the models: the R-square value (R^2) and the root mean square error (RMSE). The aim of this study was to recognize the narrow differences between the morphology of clones from the same varieties.

3.2.1. Plant material and sampling

For Pinot Gris, 105 bunches of grapes (*Vitis vinifera*) from 17 clones were manually collected in 2020 from a varietal collection vineyard in the Veneto region in Cimadolmo (TV). For Pinot Noir, 33 bunches of grapes (*Vitis vinifera*) from 6 clones were gathered in 2021 from a varietal collection vineyard in San Michele all' Adige in the Trentino province. All the Pinot grapes were collected at the "Berry ripe for harvest" phenological stage. To evaluate the severity of the grey mould, 150 numbers of grapes of Pinot Gris were sampled in each clone. Based on how much the surface of the grape was covered by

mould, the grapes were rated using a scale ranging from 0 to 3, which 0 means no symptoms, 1 means from 1 to 25%, 2 means from 26 to 50%, and 3 means more than 50% having symptoms. Then, the Townsend – Heuberger (Towsend 1943) index was computed following Equation 1, giving a score to each clone. Therefore, Pinot Gris clones were classified in different levels of grey mould severity as suggested by STURGES (Sturges 1926) by Equation 2. The Laimburg Research Centre from San Michele all' Adige assessed the Pinot Noir based on their historical data. The clones were classified from 0 to 10 ordered by resistance against *Botrytis cinerea*.

Based on OIV standard wings, height, width, shape, and average berries weight of grapes were measured. The weight of the grapes was measured, and the volume was calculated with the water displacement method.

$$TH = \frac{\sum(Ni*Vi)}{N*V} \quad \text{Eq.1}$$

TH= Townsend – Heuberger index

Ni= number of grapes in each class

Vi= class of grey mould infection ranged from 0 to 3

N= total sampled grapes

V= highest class value

$$C = 1 + \frac{10}{3}* \ log\ log\ N \quad \text{Eq.2}$$

C= Optimal class number

N= Number of samples

3.2.2. Image acquisition

For image acquisition and the 3D model reconstruction, 7 ripe grapes were collected from each clone at the harvest time in August 2020. Applying a camera Nikon D5100 (Nikon Corporation, Tokyo, Japan), having a focal length of 35mm, photos of each grape were taken. Images were acquired under laboratory conditions in a dark room lighted by neon and LED lights. The camera captured colored photos at 24-bit, 4928x3264 pixels of resolution and saved the photos in JPG format. The grapes were hanging while the camera was mounted to a special device built to turn around the target at a constant rotation speed. The device maintained 45cm between the camera and the target. The camera took a picture every two seconds thanks to the multi-shot function while rotating.

The rotation speed was set to take 33 images per rotation. The camera was mounted at three different positions. The first position was perpendicular to the grape's vertical axis, the other two at +45° and -45° to obtain a complete representation of the grape. Totally, for each grape 99 images were captured. The background was excluded with a white panel behind the grape. The image acquisition processes can be seen in Figure 3.1.

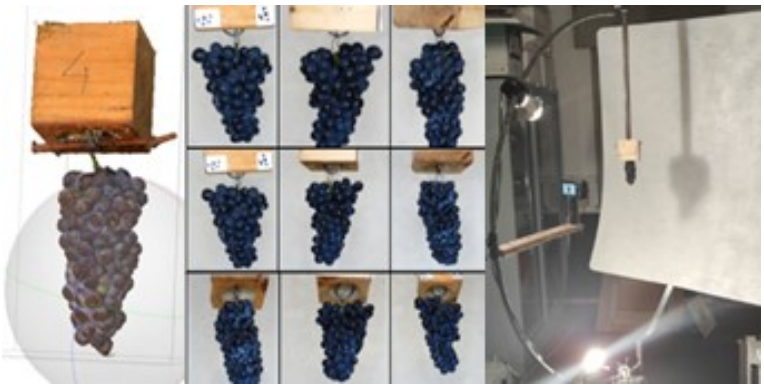

Figure 3.1. Image acquisition device, photos sequence, and final 3D virtual model.

Table 3.3. The table indicates the mean values extracted from the images of Pinot Gris. In column shape, the abbreviation includes **C**: cylindric shape, **F**: funnel shape, and **CF**: grapes with both shapes. In the TH column, the lower values mean low grey mould infections while higher values mean strong infections.

Clone	Samples number	Wings	Shape	Weight (g)	Volume (cm3)	Height (cm)	Width (cm)	Berries number	TH
FENDIT 13-CSG	6	1.00	C	149.40	141.7	14.0	10.4	109.7	14.89
VCR-5	6	1.00	C	166.25	163.3	12.1	8.7	97.7	13.78
H-1	7	1.00	C	213.59	192.9	13.3	9.1	76.9	13.33
B 10	7	1.00	C	178.89	174.3	12.4	8.1	112.7	12.67
ERSA FVG 151	6	1.00	C	147.55	136.7	14.0	9.5	111.9	12.44
CRAVIT ERSA 152	5	1.00	CF	166.54	150.0	14.4	7.4	101.9	11.56
ISMA AVIT 513	4	1.00	CF	149.08	142.5	12.1	11.0	129.3	11.56
ENTAV 53	7	1.00	C	172.49	157.1	12.6	8.1	98.1	11.11
R 6	5	1.00	C	172.15	155.0	12.9	7.8	103.8	10.44
2-15 GM	7	1.00	C	178.34	170.0	12.2	8.1	117.0	9.78
SMA 514	7	1.43	CF	189.69	172.9	13.4	13.2	96.7	9.11
ISV-F1 TOPPANI	7	1.00	C	168.80	158.6	12.2	8.1	102.2	8.44
ENTAV 457	7	1.00	CF	186.66	180.0	14.1	7.5	101.3	8.00
FR 49-207	7	1.00	F	234.57	221.0	15.0	6.8	109.1	7.33
ENTAV 52	5	1.00	F	203.40	184.0	15.0	7.8	110.6	6.89
SMA 505	7	1.00	C	161.44	155.7	12.8	7.9	101.8	6.67
1 GM	6	1.17	F	238.00	216.7	16.3	6.9	140.4	4.44

Table 3.4. The table indicates the mean values extracted from the images of Pinot Noir. In column shape, the abbreviation includes **C**: cylindric shape, **F**: funnel shape, and **CF**: grapes with both shapes. In column Botrytis Class, resistance to the pathogen is ranged from 6 to 9 where 9 means the most resistant while 6 means the most susceptible.

Clone	Samples number	Wings	Shape	Weight (g)	Volume (cm3)	Height (cm)	Width (cm)	Berries number	Botrytis Class
165	6	1.00	FC	405.97	131.67	12.93	8.00	93.0	7
583	6	1.00	C	114.77	131.67	12.44	7.62	96.5	8
667	4	1.00	C	209.73	192.50	14.71	8.04	102.6	7
828	5	1.00	C	211.84	178.00	14.05	8.60	109.4	6
GM-2013	6	2.00	C	171.77	148.33	13.88	10.89	115.3	9
SMA-201	6	1.00	C	146.10	123.33	12.74	7.82	92.7	6

3.2.3. 3D model reconstruction

Metashape 1.7.2 (Agisoft LLC) is software to build the 3D model of taken photos. It could make the object and spatial 3D models from motion photogrammetry of digital images. In this study, the software was used for the 3D models of grape images. A wood cube was captured and rebuilt with the grape. The wood cube was useful to dimension the grapes. Finally, the models were manually cleaned, deleting the noise from the background and the cube. Each image was saved in PLY format.

For each image of the grape, five horizontal sections perpendicular to the grape's vertical axis were extracted in CloudCompare. The surface and the whole volume of each grape were measured. The section cut the grape at 16.67%, 33.33%, 50%, 66.67%, and 83.33% of the grape's height, respectively. Two vertical sections were extracted, the first was positioned according to the grape's maximum width, while the second was perpendicular to the first one. Sections were saved in dxf geometry format. Autocad 2022.1 (Autodesk) was used to measure the perimeter, area, and axes length, and to draw the circumscribed circle of the horizontal sections. According to the grape's maximum width, the second was perpendicular to the first. Sections were saved in dxf geometry format. In addition, the circumscribed circle of all the horizontal sections was drawn. The native measures were saved in an Excel file and 82 native indexes, and 103 indexes were measured from each grape image (Table 3.5.).

Table 3.5. The table shows all the natives and indexes measured for each grape. The first column indicates the abbreviation of measures and indexes. The second column named reference highlights the citation and "***" means which measures were proposed in this study. The "Object" column presents which object was measured, "H" means horizontal section, "V" means vertical sections, "3D" means the grape's model, and grape means the original grape.

Measure	Reference	Formula	Object	Description
Natives				
P	(Wirth 2004)		H,V	Perimeter of vertical or horizontal Section
A	(Wirth 2004)		H,V	Area vertical or horizontal Section
Cm	(Bribiesca 2008)		H	Median circumference has the same area as the horizontal section.
PCcirc	(Li et al. n.d.)		H	Perimeter of the smallest circumference containing the section
ACcirc	(Li et al. n.d.)		H	Area of the smallest circumference containing the section
øCcirc	(Li et al. n.d.)		H	Diameter of the smallest circumference containing the section
Mja	(Wirth 2004)		H	Major axis is the longest line that can be drawn inside a horizontal section
mna	(Wirth 2004)		H	Minor axis is the longest perpendicular line to the major axis that can drown thought each horizontal section
D_P	***	Ps - P50%	H	Difference between each section's perimeter and the middle section's perimeter
D_A	***	As - A50%	H	Difference between each section's area and the middle section's area
H	OIV		V,3D	Height of grapes and vertical sections
W	OIV		V,3D	Width of grapes (W) and vertical sections (Wx, Wz)
BV	***	H*Wx*Wz	3D	Volume of the grape's bounding box
BS	***	BH∗Wx+H∗Wz+Wz∗Wx	3D	Surface of the grape's bounding box
3DV	***		3D	Volume of the 3D model retrieved by CloudCompare
Wgt	OIV		Grape	Grape weight
AcV	OIV		Grape	Actual volume of grapes measured with the water displacement method
Evol	***	3DV-ApVol	3D	Empty volume is obtained by the difference between the computed and the actual grape's volume.

S	***	3D	Surface of 3D model retrieved by CloudCompare
NB	***	H	Number of berries in the middle horizontal section
CJ	***	H	Volume of the cone containing the whole grape
ABW	OIV	Grape	Average berries weight (g)
BB	***	Grape	Berries per grape

Indexes

AP	(Cubero et al. 2015)	A/P	H,V	Ratio between area and perimeter both of sections
PA	(Li et al. n.d.)	P/A	H,V	Ratio between perimeter and area of sections
EC	(D. Zhang and Lu 2004)	Mja/mna	H	Axis ratio
Pac	***	P/Cm	H	Ratio between the section perimeter and the area of the median circumference
Apc	***	A/Cm	H	Ratio between the area of the section and the perimeter of the median section
CFS	(Cubero et al. 2015)	(P^2/A)/π	H,V	Ratio between the horizontal perimeter and area, circle = 4. Higher values mean more compactness.
RD	(Li et al. n.d.), (Bribiesca 2008; Cubero et al. 2015)	(4*π*A)/P	H	Ratio between the horizontal area and perimeter, circle has the highest value =1, values closer to 1 mean more compactness.
Cdcm	(Li et al. n.d.)	A/Asc	H	Ratio between the horizontal section area and the area of the smallest circumference containing the section
Comp	(Bribiesca 2008)	Cm/P	H	Ratio between the perimeter of the median circumference and the section's perimeter.
A/ACisop	***	$A/\pi*(P/2\pi)^2$	H	Ratio between the area of the horizontal section and the area of the circumference having the same section's perimeter.
RAr	(Chen et al. 2018)	A/(H*W)	V	Ratio between vertical section area and the area of the smallest rectangle containing the section.
Ps/P50%	***	P/P0.5	H	Ratio between each section's perimeter and the middle section's perimeter
Aa/A50%	***	A/A0.5	H	Ratio between each section area and the middle section's area
Rr	(Chen et al. 2018)	H/W	3D	Ratio between the vertical section orthogonal dimension

P/B	***	NB/AH0.5	H	Ratio between the perimeter of the middle section and the Number of berries crossed by the same section
A/B	***	NB/AH0.5	H	Ratio between the area of the middle section and the Number of berries crossed by the same section
Cm/B	***	NB/CmH0.5	H	Ratio between the Cm of the middle section and the Number of berries crossed by the same section
Accirc/B	***	NB/ACcircH0.5	H	Ratio between the Accirc of the middle section and the Number of berries crossed by the same section
AS	Cubero et al. 2015)	Wx/H	3D	Ratio between grapes X axis width (the widest) and its height
Ef	***	EVol/3DV	3D	Ratio between the empty volume and computed volume
VRr	***	3DV/BV	3D	Ratio between the grape's volume and the volume of the smallest solid containing the whole grape
VCr	***	3DV/π*H*(Wx/2)^2	3D	Ratio between the grape's volume and the volume of the smallest cylinder containing the whole grape
Rpr	***	S/BS	3D	Ratio between the grape surface and the surface of the smallest bounding box the whole grape
Cvol	***	S/V	3D	Grape surface and volume ratio, values retrieved by CC, perfect cube =1.
D	OIV	Wgt/AcV	Grape	Ratio between the grape's weight and apparent volume. Weight was measured by hand
AcVH	OIV	3DV/H	3D	Ratio between the grape's apparent volume and height
3DV/H	***	3DV/H	3D	Ratio between the 3D model's volume and height
SH	***	S/H	3D	Ratio between the 3D model's surface and height
D_CJ_3DV	***	CJ-3DV	3D	Difference between the volume of the cone containing the grape and the 3D model's volume
R_CJ_3DV	***	CJ/3DV	3D	Ratio between the volume of the cone containing the grape and the 3D model's volume
S_CJ	***	S/CJ	3D	Ratio between the 3D model's surface and the volume of the cone containing the grape
E_TotB	***	Evol/TotB	3D	Ratio between the grape's empty volume and the volume of the cone containing the grape

CJ_TotB	***	CJ/TotB	3D	Ratio between the volume of the cone containing the grape and total grape's berries
STotB	***	S/TotB	3D	Ratio between the 3D model's surface and the total berries

CloudCompare is an open-source and 3D point cloud processing software. (https://www.cloudcompare.org/main.html) that applied to making the sections from the images.

For each image of the clone, the following steps were performed.

In CloudCompare the models in PLY format were opened and zoomed on it. Then in a fixed vertical view of the cluster, the analysis started. For horizontal multiple *cross-sections*, the mesh and then *cross-section* tools were selected. By changing the bounding box border for each side and regulating it, the x, y, and z values were measured (Figure 3.2.). Tried not to change the original orientation of the bounding box because it was based on the natural gravity orientation of the grapes. And it could be possible to analyze the grapes in the same manner.

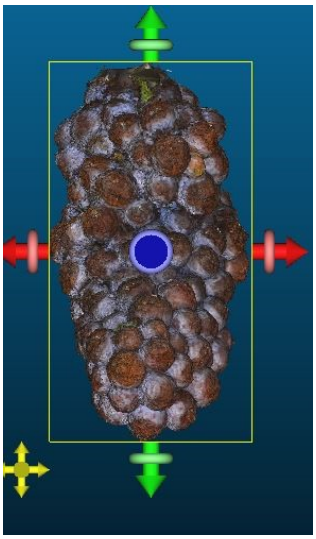

Figure 3.2. Measuring the x, y, and z values with a bounding box border

3.2.3.1. Extracting the horizontal Sections

After extracting the y value, the slice cloud or mesh was determined by the *cross-section* tool. When some extra points were found, for better analysis, these points were removed because they are noisy points from the 3D model building (Figure. 3.3.).

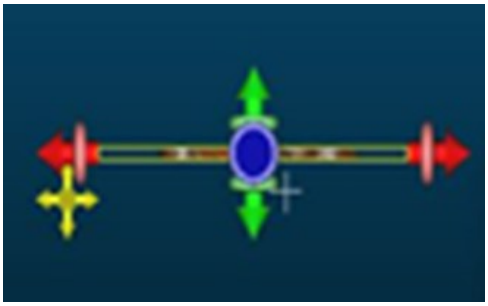

Figure 3.3. Extracting the section

This section cut the grape at 16.67%, 33.33%, 50%, 66.67%, and 83.33% of the grape's height, respectively. To extract these five sections of the horizontal level, first, the Y dimension was checked and then the envelopes were extracted. (Figure 3.4)

Saving the contour, the horizontal envelopes were prepared.

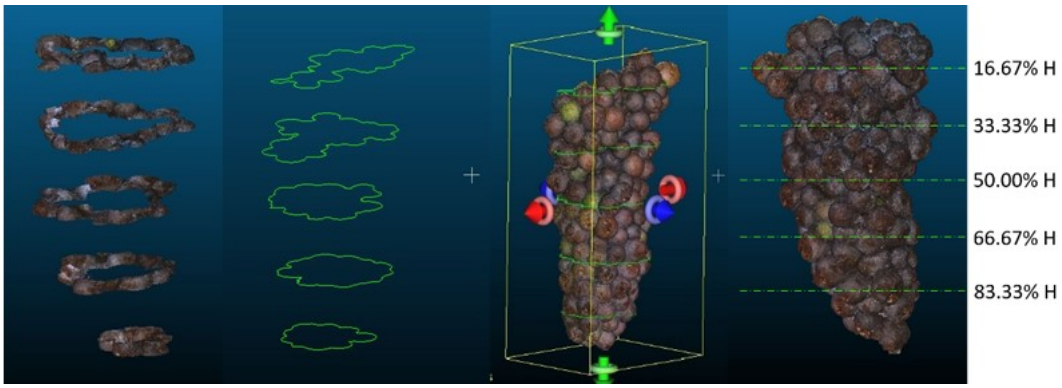

Figure 3.4. Extracting the five horizontal sections.

3.2.3.2. Extracting the vertical sections

For extracting the vertical sections, first, the original Mesh of the grape from the table of content was selected then, with the *cross-section* tool, the X width in the box thickness at 0.003 was reduced, and then, in the slice box, the new cloud was created. The new width must contain all the grapes along the X dimension. This process was repeated for the Z-dimension width at 0.003 (Figure 3.5.).

The envelopes of horizontal and vertical sections were saved in dxf extension for the next steps in AutoCad. The volume and surface values of the bunch of grapes were measured in the CloudCompare and the data were collected.

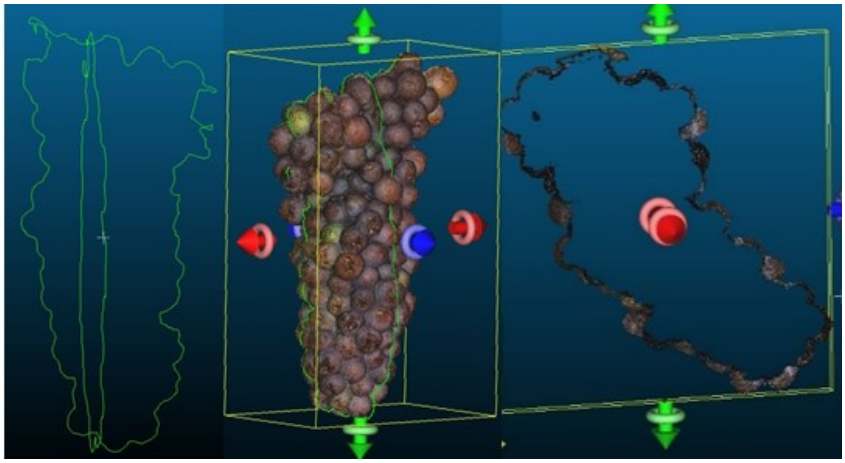

Figure 3.5. Extracting the vertical sections.

3.2.4. Measurements of the sections on AutoCad

AutoCAD (Autodesk) is a computer-aided design software. It allows you to draw and edit digital 2D and 3D designs quickly. After loading the horizontal *cross-section* file from CloudCompare, the picture appeared like this (Figure 3.6). Files were loaded and appeared in this form. By changing the point of view, it was possible to see the five *cross-sections* from one side. The sections were moved to the vertical axis (Figure 3.7).

Figure 3.6. Horizontal sections in AutoCad.

Figure 3.7. Moving the sections.

When the sections were rotated, it could be important to check the first and last sections with the images in CloudCompare (Figure 3.8.).

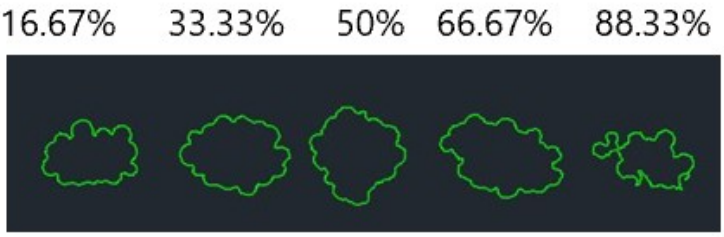

Figure 3.8. Rotating the sections. The order of sections from left includes the first, second, third, fourth and fifth sections are 16.67%, 33.33, 50%, 66.67%, and 88.33% of the grape's height respectively.

In Autocad the objects were converted into 2D (X and Y axis) flat pictures by the function *flattened* for each section. The images were made 100 times bigger and then scaled. For each horizontal section, the values for area and perimeter were extracted. Then, the longest axis in each horizontal *cross-section* was drawn by line command. It was possible to draw some lines and then choose the longest axis perpendicular to the longest shape axis (Figure 3.9.).

Figure 3.9. The longest axis in horizontal *cross-section*.

The next step was to find the smallest external circumference as seen in Figure 3.9. The value for the longest axis and smallest external circumference were extracted. For Vertical X and Z sections, the maximum height and maximum width were measured by the *Quote* tool by selecting the highest and the lowest points on the X section. This step was repeated to measure the distance between the most right and the most left points.

This way was used also for the Z section. The measures included perimeter and area information of each section plus the values of the max height and max width were collected (Figure 3.10.).

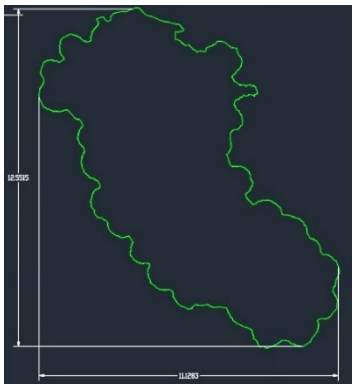

Figure 3.10. Measuring the maximum height and maximum width for vertical sections.

Finally, the number of berries for 50% of the height of the grape horizontal section of each image were counted. The picture shows an example of five horizontal middle sections of different clones. For example, in clone 1 GM 10 berries were counted and the section's perimeter measured 21.53195, while for clone HAUSER-1 11 berries were counted, and the section's perimeter measured 9.788377. Therefore, the value for descriptor berries per perimeter were 0.479907 and 1.138376 for clones 1 GM and HAUSER-1 respectively. (Figure 3.11. and table 3.6.).

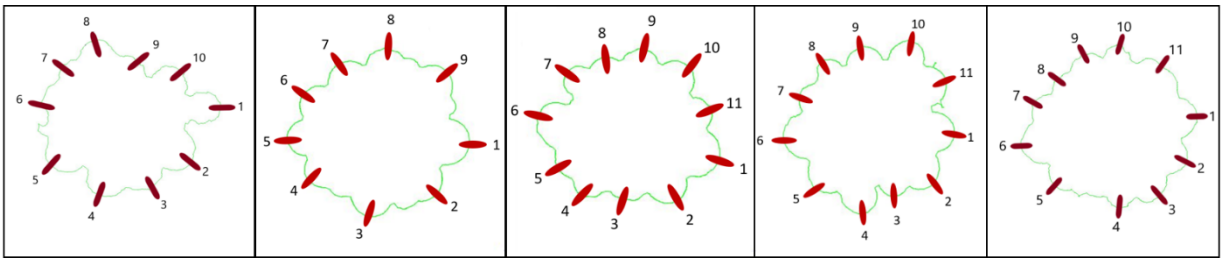

Figure 3.11. Counting the number of berries in the middle section clones 50% of the grape's height. From left the images include middle section of clones 1-GM, ISV-F1-TOPPANI, SMA-514, ERSA-FVG-151, and HAUSER-1.

Table 3.6. Calculation Berries/P for each clone.

Clones	Berriers/P	N° of berries	P (mm)
1-GM	0,48	10,33	22,4098
2-15-GM	0,56	11,43	18,9585
457F	0,48	10,29	21,7272
52-F	0,55	11,20	20,5493
53-F	0,56	12,14	21,5908
B-10-H	0,56	11,71	21,0977
CRAVIT-ERSA-152	0,51	10,60	20,8928
ERSA-FVG-151	2,95	10,67	20,0579
F13-CSG	0,77	10,67	20,6328
FR-49-207	0,51	11,14	21,8965
HAUSER-1	1,14	11,14	22,2738
ISMA-AVIT 513	0,54	11,00	20,3242
ISV-F1-TOPPANI	0,51	10,71	21,1723
R6-12	0,54	11,00	20,2611
SMA-510	0,60	11,29	18,9650
SMA-514	0,45	10,33	20,3755
VCR-5	0,51	11,17	21,9570

3.2.5. Statistical analysis

Rstudio (version 1.2.1335 © 2009-2019 RStudio) is an integrated development environment (IDE) for R. It includes a console and syntax-highlighting editor that supports direct code execution, as well as tools for plotting, history, debugging, and workspace management. In the first step, Principal Component Analysis (PCA) was applied on natives and indexes separately to understand which variable features were the most effective features. It has been decided to proceed with the PCA because it is a statistical procedure that allowed to summarize of the information contained in large data tables by means of a smaller set of “summary indices” that could be more easily visualized and analyzed. The loadings value of each variable was compared among the first components explaining at least 88% of the total variance.

In the next step, the Autocorrelation matrix was computed to detect the most auto-correlated variable. It means to find the features that were related to each other and changed according to an associated one. Multiple linear models (MLR) were applied to assess the correlation between some variable features and the grey mould severity. The

variable features related to the morphology of the grape bunch demonstrated the most correlation with the grey mould infection risk.

Two models were proposed in this study. The first model included only information considering from a bunch evaluation or 2D image analysis techniques such as height, width, number of berries, and section width. However, the second model included information from the third dimension (3D) such as the volume, the surface, the section axes and area, the berries, and the perimeter of the section.

The maximum number of features that showed a significant contribution to the model were considered (p-value ≤0.5). Because disease severity was available as the clone mean, all the grapes' features were averaged among the same clone for the regression study. In the last step, comparing the model's square regression coefficient (R^2) and the root mean square error (RMSE) was performed. Because the grey mould severity was strictly related to the compactness of the bunch, it has been considered the pattern to reveal which traits could describe the grape compactness.

Chapter 4
Experimental Analysis

4.1. Result

4.1.1. Weather condition

Analyzing the weather data recorded by the closest Arpav weather station during the vintage 2020 compared to the historical data between 1994 and 2019 years, it indicated the mean temperature in August and September of 2020 (24.6°C and 20.4°C respectively) was greater than the historical trend (22.9°C and 18.3°C respectively). In addition, the summer of 2020 had more precipitation than the historical trend (for instance, in August 2020 the total rainfall was 196.6 mm compared to the amount of 103.9 mm in August the historical data. Because of it, in this year (2020) summer, *Botrytis cinerea* had more suitable conditions to make infections. As can be seen in the below table. (Table 4.1.)

Table 4.1. Monthly mean temperature and total rainfall of 2020 vintage compared to the historical data recorded by the closest Arpav weather station.

Period	Value	April	May	June	July	August	September
2020	Tm (°C)	9.9	18.2	21.2	24.0	24.6	20.4
Historical data	Tm (°C)	13.0	17.7	21.6	23.4	22.9	18.3
2020	Rainfall (mm)	27.8	118.8	204.0	100.4	196.6	119.8
Historical data	Rainfall (mm)	101.4	124.8	106.8	90.6	103.9	128.1

4.1.2. PCA method

In this study, the numbers were used to make the charts and tables easier to understand than extended names. As the PCA method was applied for the native measures, table 4.2. shows the three clones of Pinot Gris with numbers 4, 5, and 12 have the most severity class of grey mould with very high class whereas the number 8 had the lowest value for severity class with very low class. Between these two groups, there were clones classified into the high, medium, and low classes. This data was based on the

chart in Figure 4.1. indicates the score of grapes among the first and second PCA's dimensions. The first and the second dimensions explained 33.58% and 20.10% of the total variance, respectively. Clones were figured from 1 to 17 to make the chart easier to understand. Clones were divided into five classes because it was the optimal number of classes resulting from Sturge's equation.

Table 4.2. The table assigns to each clone of Pinot Gris the number and the severity class of grey mould based on the scatter plot of Pinot Gris PCA grapes' scores (Figure 4.1.)

Number	Clone	Class
4	B 10	Very High
5	H-1	Very High
12	VCR-5	Very High
14	FENDIT 13-CSG	Very High
9	CRAVIT ERSA 152	High
13	ERSA FVG 151	High
15	ENTAV 53	High
17	ISMA-AVIT 513	High
2	2-15 GM	Medium
6	R 6	Medium
10	SMA 514	Medium
1	ENTAV 457	Low
3	SMA 505	Low
7	ENTAV 52	Low
11	ISV-F1 TOPPANI	Low
16	FR 49-207	Low
8	1 GM	Very Low

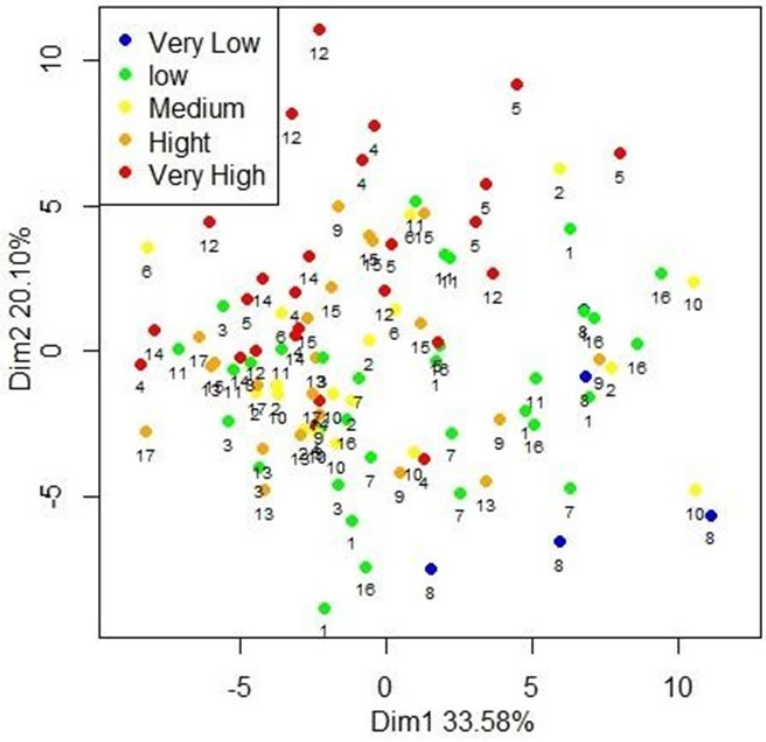

Figure 4.1. This scatter plot presents Pinot Gris PCA grapes' scores distributed according to dimension one, the horizontal axis, and dimension two, the vertical axis. The points represent all the grapes sampled. The numbers indicate the clone. The clone's name and number are listed in table 4.2. The color indicates the severity class. Numbers 33.58% and 20.10% represent the portion of total variance explained by the first and the second PCA dimensions.

For Pinot Noir after applying the PCA on the native measures, clone number 4 of Pinot Noir had the highest resistance to grey mould with very high class whereas numbers 5 and 3 had a low resistance class against grey mould. Between these two groups, there were clones classified into the high, and medium classes. As verified in Pinot Gris, the clones of the lowest and the highest class occupied opposite corners.

Table 4.3. The table indicates for each clone of Pinot Noir the number and the resistance class against grey mould based on the scatter plot of Pinot Noir PCA grapes' scores (Figure 4.2.)

Number	Clone	Class
4	GM-2013	Very High
2	583	High
6	667	Medium
1	165	Medium
5	SMA-201	Low
3	828	Low

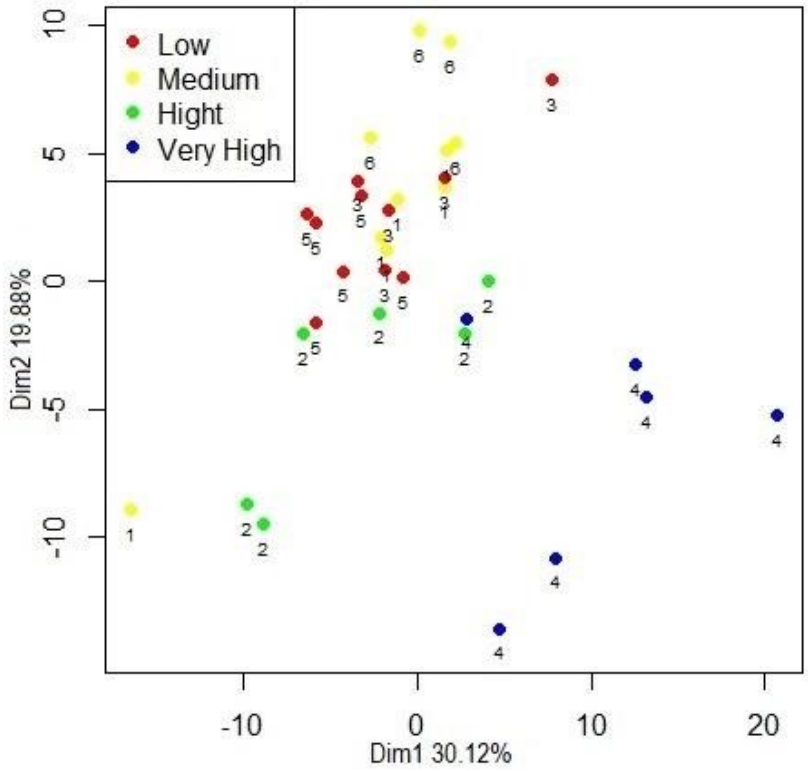

Figure 4.2. This scatter plot presents Pinot Noir PCA grapes' scores distributed according to dimension one, the horizontal axis, and dimension two, the vertical axis. The points represent all the grapes sampled. The numbers indicate the clone. The clone's name and number are listed in table 4.3. The Colour indicates the resistance class against grey mould. The percentages 30.12% and 19.88% represent the portion of total variance explained by the first and the second PCA dimensions.

4.1.3. MLR model

Considering the 2D regression model, only the features related to 2D were assessed. These features were such as descriptors of shape and compactness from the images.

However, the 3D regression model used all 2D information and the information of section analysis, volume, surface, and the combination of data.

The next step was the MLR. To describe the MLR just five descriptors were sufficient, and more descriptors did not make a significant effect on statistical analysis. Equations 3 and 4 reported 2D and 3D models. When the 3D MLR replaced the 2D MLR, the regression changed from 0.656 to 0.838, and based on RMSE, decreased from 1.713 to 1.175, the accuracy of estimation was enhanced.

In these equations, Branching, and MaxW related to the presence of the wings while Empty volume reported the difference between the total volume inside the 3D model mesh and the actual volume based on the volumes of berries and rachis. Surf.H presents the ratio between the mesh surface and the height of the grape. MaxW0.5 and MaxW1 show the max width of the grape at the middle and first sections closest to the peduncle where Max.Axis_H1 and Max.Axis_H4 represent the length of the longest axis of sections one and four, at 16.67% and 66.67% of the height of the grape, respectively.

TH= -32.8236 * Branching –16.4542* MaxW0.5 +0.0743 *MaxW –0.4630* Height -0.3148* MaxW1 +655184 *Eq. 3*

TH= -4.8797* EmpF +0.4142 *Surf.H -2.4653 *P_Berries -0.6864*MaxAxis_H4 -3.8570 *MaxAxis_H1 +32.6925 *Eq. 4*

The Figure 4.3. indicates the scatter plots which demonstrate the clones among actual and predicted TH values, while the colour shows the class severity assigned to clones. The Ravaz Index was also measured as the ratio between the yield and the pruning wood weight, table 4.4.

Table 4.4. Ravaz Index is expressed as the ratio between grape yield and pruning wood weight.

Clone	Ravaz Index
H-1	4.49
CRAVIT ERSA 152	7.48
FR 49-207	7.83
ISV-F1 TOPPANI	8.19
VCR-5	8.24
R 6	9.12
ENTAV 457	9.55
ENTAV 52	10.55
FENDIT 13-CSG	11.47
B 10	11.68
ERSA FVG 151	11.79
ISMA-AVIT 513	12.14
ENTAV 53	12.22
SMA 505	12.84
SMA 514	12.87
2-15 GM	13.9
1 GM	17.29

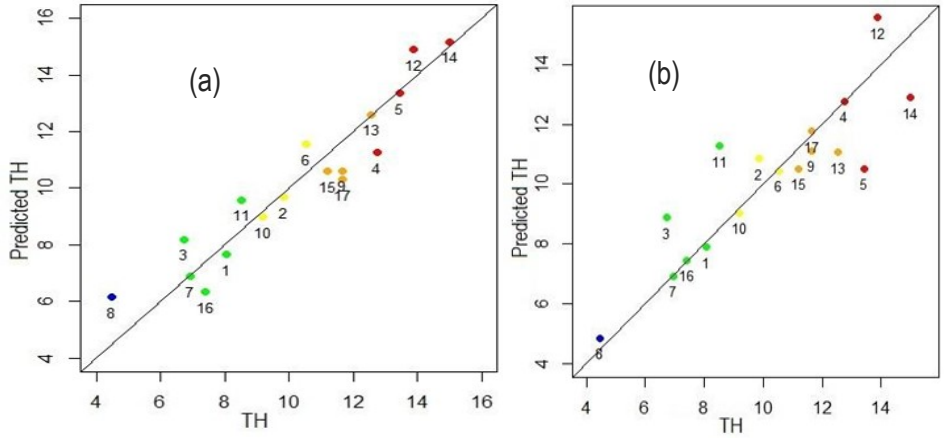

Figure 4.3. These two scatter plots show the actual and predicted TH of 2D (a) and 3D (b) MLR of Pinot Gris. The black line represents the ideal regression line with a slope value of 1, while the color of the point is referred to as the clone severity class.

For Pinot Noir, the descriptors of the 2D model did not highlight any significant from the MLR. Therefore, the MLR computed on the 3D descriptor included only three variables to avoid the overfitting of the model. As a result, the proposed MLR estimated an R^2 of 0.936 and an RMSE of 0.297.

Grey mould resistance = 8.1643 *P_Berries +0.7079 *Max.Axis_H4 +25.1527 *Surf.CJ -30.8111 Eq. 5

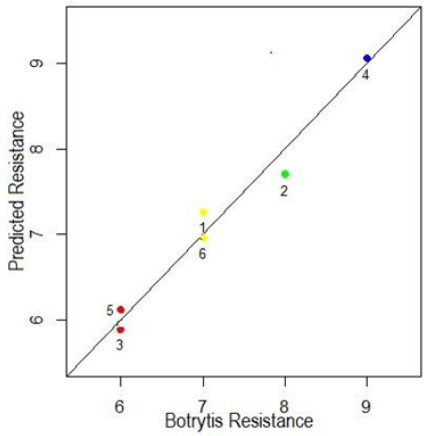

Figure 4.4. The scatter plot displays the actual and predicted resistance against the grey mould of the 3D MLR model of Pinot Noir. The black line shows the ideal regression line with a slope value of 1, while the color of the point is referred to as the clone severity class.

4.1.4. Analyzing the relationship between the descriptors and severity class

There were some descriptors that could affect the severity class of grey mould. To find the most effective ones in detail, the scatterplots were drawn based on the tables 4.5.

Table 4.5. The values of descriptors and TH value of grey mould in Pinot Gris.

Clone	TH	Height (cm)	Weight (g)	APP. Vo (cm^3)l	Surface (cm^2)	Empty Fraction	Surf/H	ABW (g)	N_Berries	Berriers/P	Surf/ Berries	Max Axis1 (mm)	Max Axis 4 (mm)
F13-CSG	14.9	14.0	149.4	141.7	350.3	0.2	25.1	1.5	109.7	0.8	3.2	6.0	5.6
VCR-5	13.8	12.1	166.3	163.3	331.2	0.1	27.3	1.5	97.7	0.5	3.4	5.2	5.7
HAUSER-1	13.3	13.3	213.6	192.9	407.3	0.2	30.7	1.6	76.9	1.1	5.3	6.5	6.1
B-10-H	12.7	12.4	178.9	174.3	328.1	0.1	26.5	1.4	112.7	0.6	2.9	6.2	5.5
ERSA-FVG-151	12.4	14.0	147.6	136.7	388.9	0.2	27.8	1.4	111.9	3.0	3.5	6.8	4.8
CRAVIT-ERSA-152	11.6	14.4	166.5	150.0	442.5	0.3	30.8	1.6	101.9	0.5	4.3	6.4	5.2
ISMA-AVIT 513	11.6	12.1	149.1	142.5	313.5	0.1	25.9	1.3	129.3	0.5	2.4	6.4	4.9
53-F	11.1	12.6	172.5	157.1	343.1	0.2	27.2	1.5	98.1	0.6	3.5	6.5	5.3
R6-12	10.4	12.9	172.2	155.0	353.6	0.2	27.4	1.5	103.8	0.5	3.4	6.0	5.4
2-15-GM	9.8	12.2	178.3	170.0	363.4	0.2	29.7	1.4	117.0	0.6	3.1	6.7	4.9
SMA-514	9.1	13.4	189.7	172.9	430.4	0.2	32.1	1.5	96.7	0.4	4.4	7.1	5.2
ISV-F1-TOPPANI	8.4	12.2	168.8	158.6	356.1	0.2	29.1	1.4	102.2	0.5	3.5	6.5	5.7
457F	8.0	14.1	186.7	180.0	477.0	0.3	33.8	1.5	101.3	0.5	4.7	7.5	5.1
FR-49-207	7.3	15.0	234.6	221.0	489.2	0.2	32.6	1.3	109.1	0.5	4.5	8.0	5.6
52-F	6.9	15.0	203.4	184.0	478.6	0.2	31.9	1.4	110.6	0.5	4.3	7.7	5.3
SMA-510	6.7	12.8	161.4	155.7	343.9	0.1	26.8	1.5	101.8	0.6	3.4	7.1	4.9
1-GM	4.4	16.3	238.0	216.7	563.1	0.2	34.4	1.3	140.4	0.5	4.0	8.1	5.0

APP.Vol: Apparent volume, **ABW_g**: Average Berry Weight N**_Berries**: number of berries, **Empty Fraction**: Ratio between the empty volume and computed volume (CC). **Surf/H:** 3D model surface/height. **Surf/Berries**: 3D model surface / total number of berries. **Berries/P**: Number of berries per section/section perimeter. **Max Axis 4**: Major axis horizontal section 4 (66.33% of the height starting from the peduncle) **Max Axis 1**: Major axis first horizontal section from the peduncle.

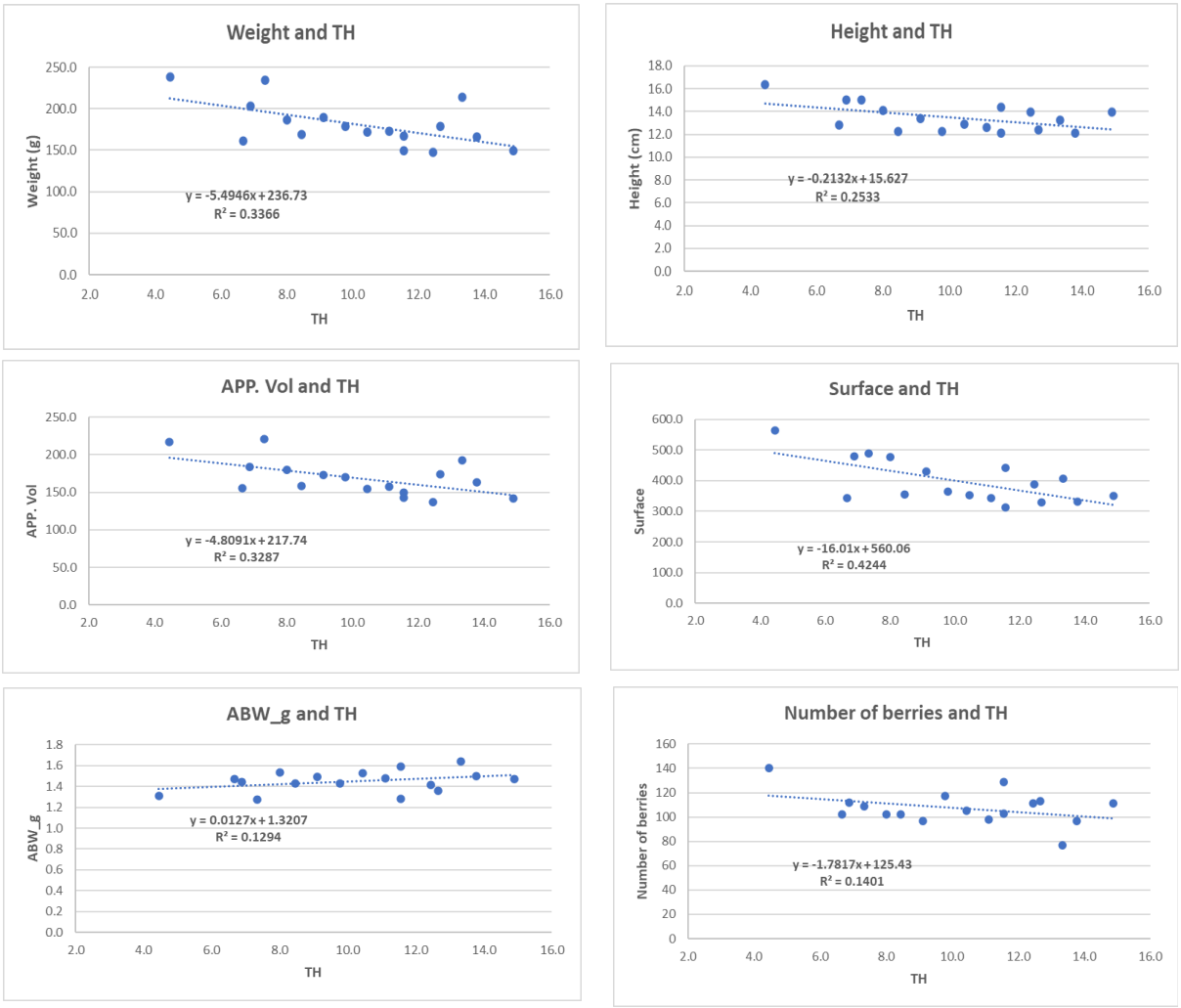

Figure 4.5. These scatterplots indicate the values of descriptors as weight, height, APP.Vol, surface, ABW_g, and Number of berries in the y-axis related to TH value of grey mould.

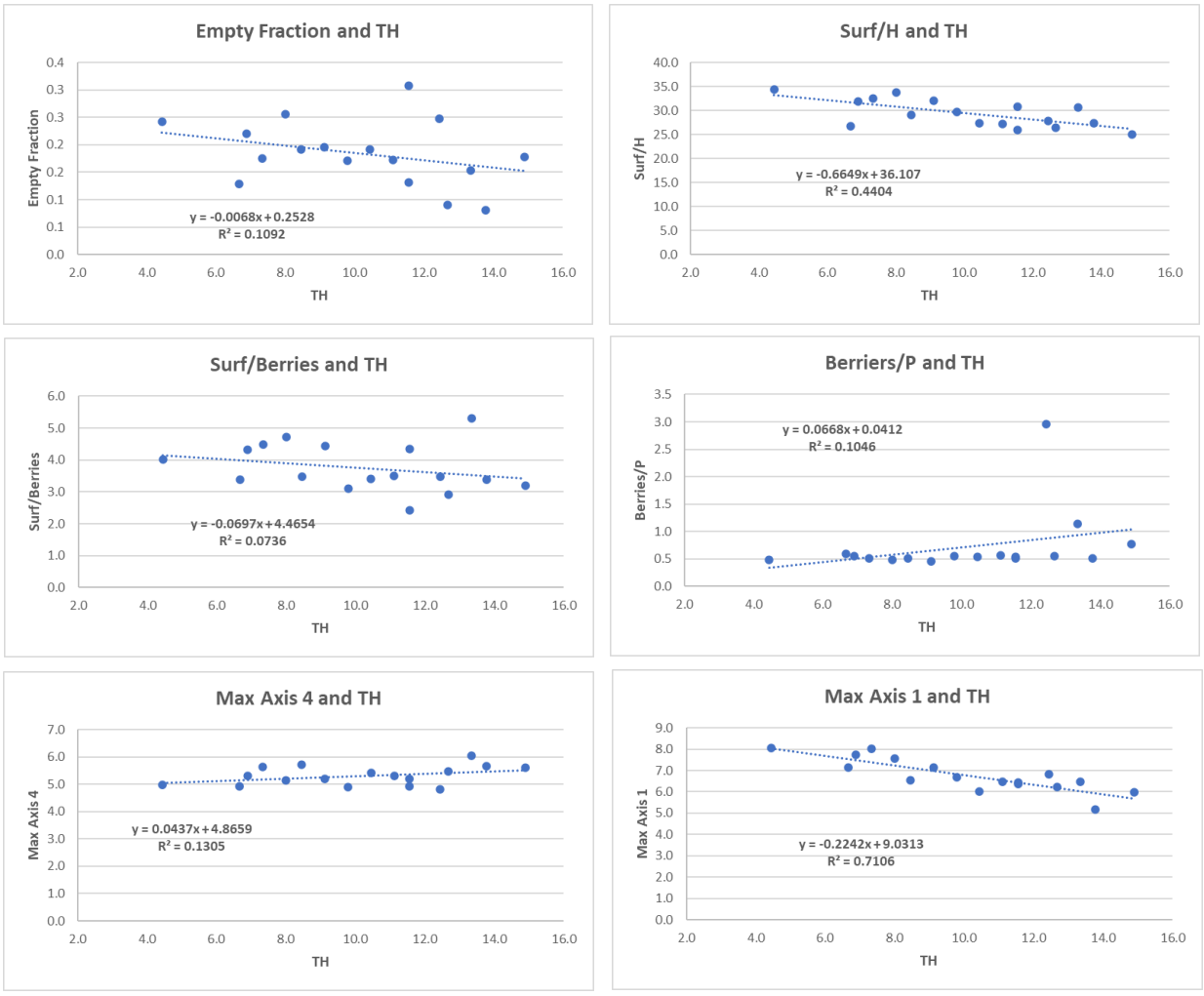

Figure 4.6. These scatterplots indicate the values of descriptors as Empty fraction, Surf/H, Surf/Berries, Berries/P, Max Axis 4, and Max Axis 1 in the y-axis related to TH value of grey mould.

These scatterplots indicated that the changes related to these features could be impressed with the TH value. These twelve descriptors did not have a high value of R^2. As seen, R^2 was between 0.07 to 0.44 for most of them. However, Max Axis 1 indicated more value which was 0.71 compared to the other factors. (Figure 4.5 and 4.6.) All descriptors had a negative correlation with TH value except the ABW_g, berries /P and Max Axis 4.

Table 4.6. The values of descriptors and severity class of grey mould in Pinot Gris.

Class	Height	Weight	APP. Vol	ABW_g	N_Berries	Surface
Very Low	16.3493	238.0000	216.6666	1.3073	140.3620	563.0736
Low	13.8367	190.9742	179.8657	1.4285	105.0169	428.9870
Medium	12.8546	180.0595	165.9523	1.4823	105.8576	382.4548
High	13.2659	158.9126	146.5773	1.4421	110.2952	371.9892
Very High	12.9339	177.0303	168.0357	1.4926	99.24988	354.2208

APP.Vol: Apparent volume, **ABW_g:** Average Berry Weight **N_Berries**: number of berries.

Figure 4.7. The above box plots show the differences between the five severity classes of grey mould for each descriptor in Pinot Gris.

Table 4.7. The values of descriptors and severity class of grey mould in Pinot Gris.

Class	Empty Fraction	Surf/H	Surf/Berries	Berriers/P	Max Axis 4	Max Axis1
Very Low	0.2417	34.4401	4.0115	0.4799	4.9882	8.0549
Low	0.1944	30.8453	4.0761	0.5276	5.3456	7.3945
Medium	0.1863	29.7217	3.6535	0.5162	5.1708	6.6222
High	0.2145	27.9296	3.4351	1.1429	5.0543	6.5251
Very High	0.1256	27.4030	3.6979	0.7444	5.7029	5.9675

Empty Fraction: Ratio between the empty volume and computed volume (CC). **Surf/H:** 3D model surface/height. **Surf/Berries**: 3D model surface / total number of berries. **Berries/P**: Number of berries per section/section perimeter. **Max Axis 4**: Major axis horizontal section 4 (66.33% of the height starting from the peduncle) **Max Axis 1**: Major axis first horizontal section from the peduncle.

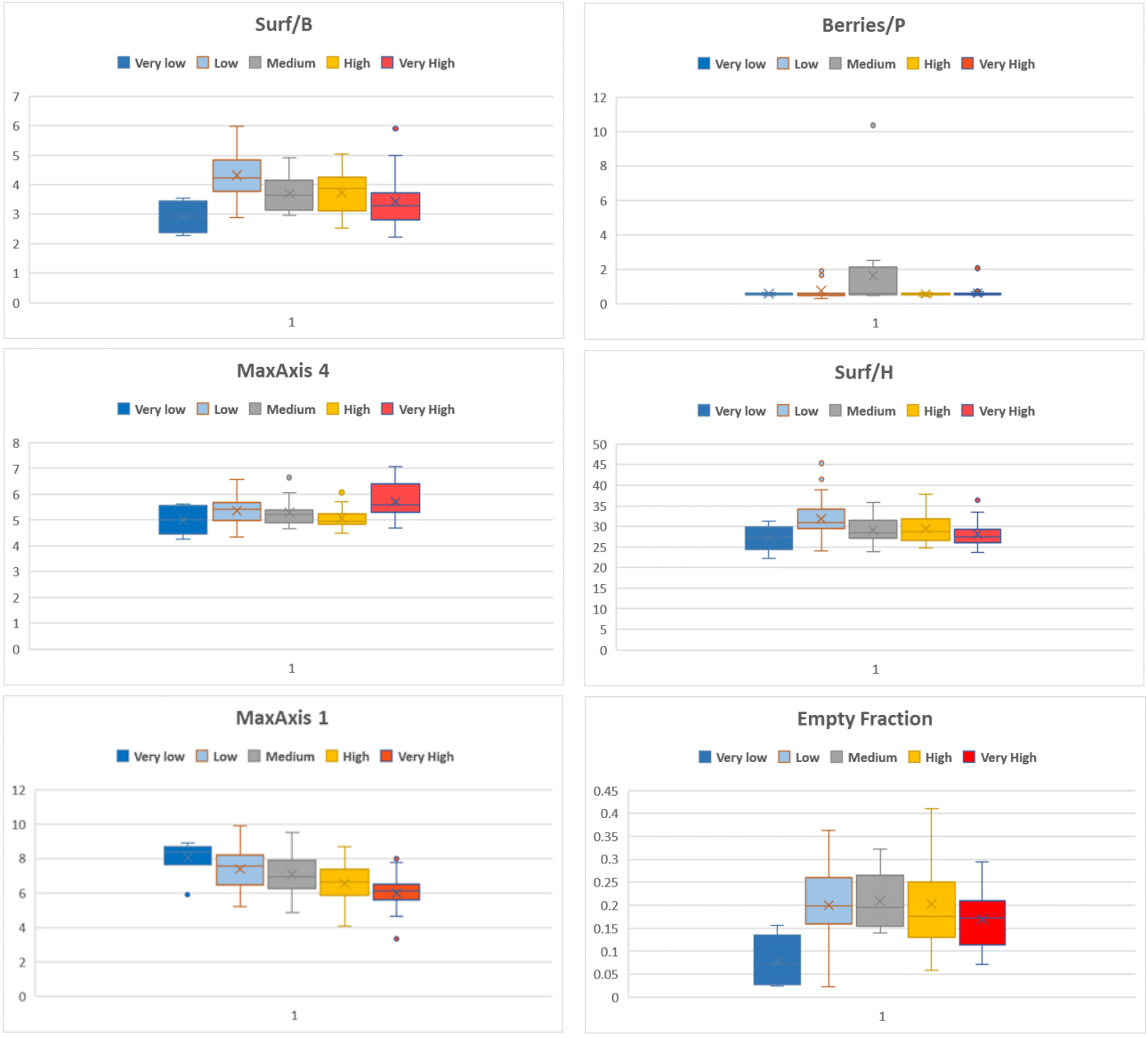

Figure 4.8. The above box plots show the differences between the five severity classes of grey mould for each descriptor in Pinot Gris.

Based on table 4.6 and 4.7 the values of descriptors and five severity classes of grey mould in Pinot Gris were analysed by the box plots (Figues 4.7. and 4.8.). It can be considered high differences in mean value of weight, height, Max Axis 1 and surface from very low to very high severity classes. In addition, it represented the trend from very low class to very high class in thses descriptors.

4.1.5. Assessing the data

In addition, the clones of Pinot Gris with different susceptibility to grey mould were divided into two groups to find the differences between the two group and their features. The clones with higher values than 10 for TH in the first group and the clones with lower values than 10 in the second group were arranged however the clone R6 with 10.44 was present in both tables. Two tables were created and the relation between the two groups for each feature was assessed.

Table 4.8. The two groups of clones of Pinot Gris with high and low susceptibility to grey mould

Clone Group 1	**Samples number**	**Wings**	**Shape**	**Weight (g)**	**Volume (cm3)**	**Height (cm)**	**Width (cm)**	**Berries number**	**TH**
FENDIT 13-CSG	6	1	C	149.4	141.7	14	10.4	109.7	14.89
VCR-5	6	1	C	166.25	163.3	12.1	8.7	97.7	13.78
H-1	7	1	C	213.59	192.9	13.3	9.1	76.9	13.33
B 10	7	1	C	178.89	174.3	12.4	8.1	112.7	12.67
ERSA FVG 151	6	1	C	147.55	136.7	14	9.5	111.9	12.44
CRAVIT ERSA 152	5	1	CF	166.54	150	14.4	7.4	101.9	11.56
ISMA AVIT 513	4	1	CF	149.08	142.5	12.1	11	129.3	11.56
ENTAV 53	7	1	C	172.49	157.1	12.6	8.1	98.1	11.11
R 6	5	1	C	172.15	155	12.9	7.8	103.8	10.44

Clone Group 2	**Samples number**	**Wings**	**Shape**	**Weight (g)**	**Volume (cm3)**	**Height (cm)**	**Width (cm)**	**Berries number**	**TH**
R 6	5	1	C	172.15	155	12.9	7.8	103.8	10.44
2-15 GM	7	1	C	178.34	170	12.2	8.1	117	9.78
SMA 514	7	1.43	CF	189.69	172.9	13.4	13.2	96.7	9.11
ISV-F1 TOPPANI	7	1	C	168.8	158.6	12.2	8.1	102.2	8.44
ENTAV 457	7	1	CF	186.66	180	14.1	7.5	101.3	8.00
FR 49-207	7	1	F	234.57	221	15	6.8	109.1	7.33
ENTAV 52	5	1	F	203.4	184	15	7.8	110.6	6.89
SMA 505	7	1	C	161.44	155.7	12.8	7.9	101.8	6.67
1 GM	6	1.17	F	238	216.7	16.3	6.9	140.4	4.44

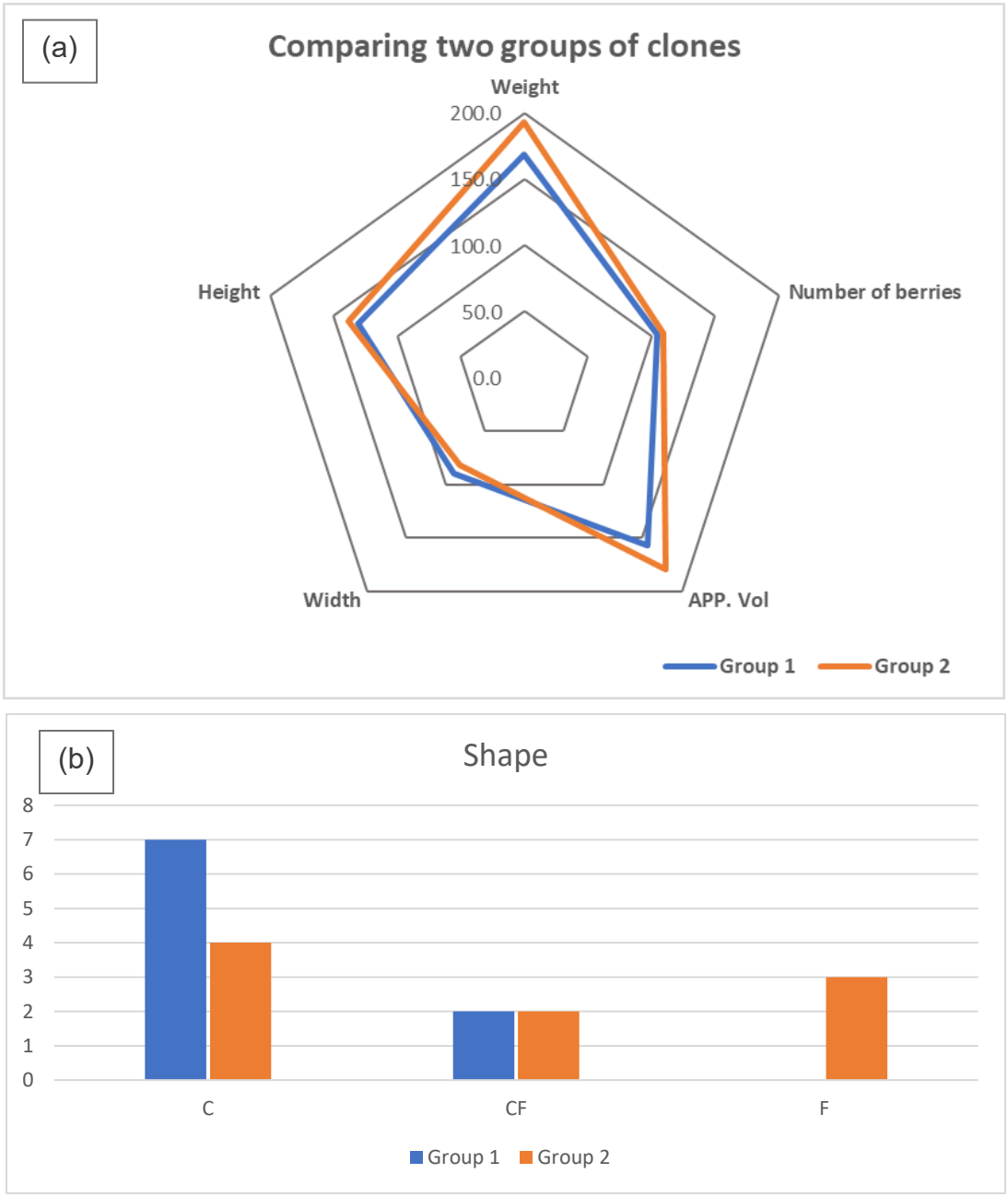

Figure 4.9. These graphs indicate the difference between two groups of clones of Pinot Gris with high and low susceptibility to grey mould. In graph (a) the mean value of five factors were analyzed for two groups (the scale of the mean values for the weight, height, width, and volume were g, mm, mm, cm^2). The histogram (b) reassumes the clones' shapes by the two groups. The blue line presents group one, and the orange line shows group two. **C**: cylindric shape, **F**: funnel shape, and **CF**: grapes with both shapes.

In the graph, for the weight, volume, height, and the number of berries, group two showed more values in most clones than group one. Only for the width the values of group one showed the higher numbers. As seen in the bar charts, in group one there were seven cylindrical shape clones and two with both shapes whereas in group two there were four cylindrical shape clones, two with both shapes, and three funnel shapes which was the difference between the two groups.

Figure 4.10. These box plots present the differences between two groups for six factors weight, volume, height, width, number of berries and the number of wings.

Table 4.9. This table shows the statistical analysis related to two groups of Pinot Gris clones. In P_value column, the signs mean "*" for P.value<0.05 and n.s. for for P.value > 0.05.

Descriptor	Average	Standard deviation	Number of bunches per group	P-value
weight 1	168.4378	19.3219	48	*
weight 2	192.5611	26.1235	53	
height 1	13.0889	0.8252	48	n.s.
height 2	13.7667	1.3457	53	
volume 1	157.0556	16.7902	48	*
volume 2	179.3222	23.2465	53	
width 1	8.9000	1.1470	48	n.s.
width 2	8.2333	1.8123	53	
number of berries 1	104.6667	13.4166	48	n.s.
number of berries 2	109.2111	12.4179	53	
wings 1	1.0000	0.0000	48	n.s.
wings 2	1.0667	0.1390	53	

Table 4.9. reported the result of the statistical analysis of the two groups with Anova for the non-normal distribution sample. The weight and the volume showed significant and meaningful differences while the differences between the other factors were not significant. These results were confirmed by box plots (Figure 4.10). In these box plots the weight, and volume represented the more variability of data for the group two than the group one and for most of the descriptors, the mean value of group two was more than mean value of the group one.

These steps were performed for Pinot Noir clones. However, splitting the number of Pinot Noir bunches into two groups did not generate enough data for statistical analysis.

4.2. Discussion

Considering the OIV standard descriptors, finding a strong relationship between the features of Pinot clones and the severity of grey mould was unclear. Because all the grapes were from the same grapevine variety and very similar to each other. Most of the grapes were compact and cylindric without wings and just a few of them had branching from the main grape's body. Therefore, it is needed to assess more details to find the differences between the clones.

The analysis with the PCA model and score plotting the result showed a diagonal trend crossing the second and the fourth quadrants both in Pinot Gris and Pinot Noir. This model was applied to native measures because indexes were defined of formulas between natives when the native measures were calculated from grapes. Based on the result, clone 1 GM of Pinot Gris indicated the lowest severity class, where whereas the highest severity class, belonged to FENDIT 13-CSG, VCR-5, and B 10. 1 GM that had a funnel shape, and some grape samples have two wings. Clone 1 GM had the highest values for height, width, empty volume, and branching that highlighted this clone had less compactness than the other clones and was less susceptible to grey mould. FENDIT 13-CSG, VCR-5, and B 10 had a shape with one wing. They had the lowest values for height, the fraction of estimated empty volume, and surface. Clones FENDIT 13-CSG, VCR-5, and B 10 could be considered very compact grapes. This result could demonstrate that with high compactness and large density of grapes, the risk of grey mould increased, and the condition was more suitable for fungi penetration to the berries. For Ravaz index, however, clone 1 GM showed the highest index value, and the linear regression between the Ravaz index and the grey mould severity was very low ($R^2 = 0.15$).

The clone GM-2013 of Pinot Noir had the highest resistance to grey mould based on the PCA analysis. This clone had two wings and a cylinder shape. In addition, it had the highest number for the width and surface. Moreover, it was the second clone for the estimated empty volume fraction and branching. Contrary to it, clones 828 and SMA-201 were the lowest resistant to grey mould and they were clustered with clone 667, which was belonged to the medium class and shows many descriptors of the middle classes. SMA-201 had the smallest value for the ratio between surface, height, volume, and berries number. Also, clone 828 had the lowest resistance to grey mould. There were some factors of the grape shape related to compactness that make the bunch resistant or susceptible to grey mould infections. The other parameters include the berry's skin thickness, the chemical content of berries juice, genetic patterns, dangerous insects, and the environment and climate. In this study also the weather condition was suitable for *Botrytis cinerea* to make infections.

For Pinot Gris, when the number of R^2 increased in the 3D MLR, the RMSE improved compared to the 2D MLR. The most important variables of the 2D MLR were the width of

sections and the presence of branching from the main body of the grapes. For 3D analysis, section width and many other exciting descriptors were added. The ratio between the perimeter of the middle section and the berries number in the middle section means the portion of the section perimeter occupied by each berry. Lower values could mean berries were tiny and compact. For example, clone 1 GM of Pinot Gris had ten berries, while clone FENDIT 13-CSG had eleven ones and a smaller perimeter than clone 1 GM. The ratio between perimeter and berries resulted higher in favour of clone 1 GM 2.0837cm and 1.78542cm, respectively. The surface of the mesh was related to the grape dimension, branching, and compactness. The berries of compact grapes often tighten and were close to each other, while the berries of loose grapes were far from each other. Consequently, the contribution of each berry in compact grapes was lower to the whole surface than in loose ones. The ratio between surface and height was an index to standardize the surface of the grape dimension. In fact, measuring the surface was limited by the quality of images and their resolution and alignment.

For Pinot Noir, the 2D analysis had no significant result with 2D descriptors to the MLR model and only three descriptors took part in the 3D MLR model. The clones of Pinot Noir grapes were much more different than the clones of Pinot Gris. Therefore, they showed significant divergence in shape, number of wings, and branching.

In this part of the study, grape weight and volume were not so relevant to predict bunch compactness and grey mould severity compared to the studies related to the indexes of compactness (J Tello and Ibáñez 2014) and evaluation of cluster length, width, and elongation by the analysis of 2D images (Javier Tello et al. 2016). In these studies, the weight and length were used to create the indexes for estimating the bunch compactness.

To find more detail about the relationship between the more effective descriptors for Pinot Gris and the severity class of grey mould the plots were designed. Among the twelve descriptors, the R^2 value for Max Axis 1 (Major axis first horizontal section from the peduncle) was 0.71. In addition, the weight, height, Max Axis 1 and surface compared to the other factors showed a higher variability of data related to severity classes of grey mould that could be presented these factors were more effective in the severity of grey mould infection on grapes. They were more related to the morphological characteristic of

the grape and were based on the surface and height of the grape which showed the importance of these factors for the presence of the infection.

In another analysis, the two groups of clones for Pinot Gris were created to find the differences between high-susceptible and low-susceptible clones of grey mould. After analysis of the graphs, some features such as the weight, volume, and wings in group two showed more values in most clones than in group one. Considering the bar charts related to the shape factor, in group one there were seven cylindrical shape clones and two with both shapes whereas in group two there are four cylindrical shape clones, two with both shapes, and three funnel shapes which was the difference between the two groups, and it could indicate the importance of the shape factor in grey mould infection. Regarding the result of the statistical analysis of the two groups the weight and the volume showed significant differences which were like the result of the graphs and confirmed the importance of these two factors between the two groups and enhancing the infection on berries.

4.3. Conclusions

The purpose of this study was to understand the factors of the grapevine morphology of grapevine clusters by extracting the data from the 3D reconstruction of grapes by photogrammetry techniques. This method compared to other methods sustainable pursued to make a deep analysis of bunches' morphology comparing intra-variety clones. Seventeen Pinot Gris clones and six Pinot Noir clones were collected to find the most compact clone. The images of grapes were processed with image software. The data was extracted from five horizontal and two vertical sections. The PCA analysis was performed on the data to find the distribution trend in the behaviour of the clones to develop grey mould infections. Two multiple linear regression models were proposed per grapevine variety considering the most important descriptors from the PCA. The first model assessed the correlation between the grey mould severity and the descriptors from the 2D analysis, while the second model analyzed both descriptors from the 2D and 3D analysis. The 3D MLR presented higher performances than the 2D MLR. In addition, analyzing the data with graphs and statistical results showed the importance of weight

and volume, and shape, besides the ratio between surface and height, empty volume, and width as important descriptors of compactness that could affect grey mould infection.

The results proved the relevance of grape morphology on grey mould infection in grapes. Further studies should be proposed on other grapevine varieties to prove the importance of the descriptors selected in this trial. It is necessary to repeat this work next year to confirm the results based on other vintages or different grapevine varieties.

Bibliography

Alessandrini, M., Calero Fuentes Rivera, R., Falaschetti, L., Pau, D., Tomaselli, V., & Turchetti, C. (2021). A grapevine leaves dataset for early detection and classification of esca disease in vineyards through machine learning. *Data in Brief*, *35*. https://doi.org/10.1016/j.dib.2021.106809

Anastasiou, E., Balafoutis, A., Darra, N., Psiroukis, V., Biniari, A., Xanthopoulos, G., & Fountas, S. (2018). Satellite and proximal sensing to estimate the yield and quality of table grapes. *Agriculture (Switzerland)*, *8*(7). https://doi.org/10.3390/agriculture8070094

Arnó, J., Martínez Casasnovas, J. A., Ribes Dasi, M., & Rosell, J. R. (2009). Review. Precision viticulture. Research topics, challenges and opportunities in site-specific vineyard management. *Spanish Journal of Agricultural Research*, *7*(4), 779. https://doi.org/10.5424/sjar/2009074-1092

Bélanger, M. C., Roger, J. M., Cartolaro, P., & Fermaud, M. (2011). Autofluorescence of grape berries following Botrytis cinerea infection. *International Journal of Remote Sensing*, *32*(14), 3835–3849. https://doi.org/10.1080/01431161003782064

Bem, B. P. de, Bogo, A., Everhart, S., Casa, R. T., Gonçalves, M. J., Filho, J. L. M., & Cunha, I. C. da. (2015). Effect of Y-trellis and vertical shoot positioning training systems on downy mildew and botrytis bunch rot of grape in highlands of southern Brazil. *Scientia Horticulturae*, *185*, 162–166. https://doi.org/10.1016/j.scienta.2015.01.023

Bendel, N., Backhaus, A., Kicherer, A., Köckerling, J., Maixner, M., Jarausch, B., et al. (2020). Detection of two different grapevine yellows in Vitis vinifera using hyperspectral imaging. *Remote Sensing*, *12*(24), 1–22. https://doi.org/10.3390/rs12244151

Bendel, N., Kicherer, A., Backhaus, A., Klück, H. C., Seiffert, U., Fischer, M., et al. (2020). Evaluating the suitability of hyper- and multispectral imaging to detect foliar symptoms of the grapevine trunk disease Esca in vineyards. *Plant Methods*, *16*(1). https://doi.org/10.1186/s13007-020-00685-3

Billard, A., Fillinger, S., Leroux, P., Bach, J., Lanen, C., Lachaise, H., et al. (2011). Fenhexamid Resistance in the Botrytis Species Complex, Responsible for Grey Mould Disease. In *Fungicides - Beneficial and Harmful Aspects*. InTech. https://doi.org/10.5772/27512

Bribiesca, E. (2008). An easy measure of compactness for 2D and 3D shapes. *Pattern Recognition*, *41*(2), 543–554. https://doi.org/10.1016/j.patcog.2007.06.029

Broome J.C., E. J. T. , M. J. J. , L. B. A. (1995). Development of an infection model for Botrytis bunch rot of grapes based on wetness duration and temperature. *Phytopathology*, *85*.

Brunetto, G., Ricachenevsky, F. K., Stefanello, L. O., de Paula, B. V., de Souza Kulmann, M. S., Tassinari, A., et al. (2020). Diagnosis and management of nutrient constraints in grape. *Fruit Crops: Diagnosis and Management of Nutrient Constraints*, 693–710. https://doi.org/10.1016/B978-0-12-818732-6.00047-2

Bryan Hed. (2016). 2016 Post Bloom Disease Management Review.

Chandrasekar Venkitasamy, Z. Pan. (2019). Grapes. *Integrated Processing Technologies for Food and Agricultural By-Products*.

Chen, X., Ding, H., Yuan, L. M., Cai, J. R., Chen, X., & Lin, Y. (2018). New approach of simultaneous, multi-perspective imaging for quantitative assessment of the compactness of grape bunches. *Australian Journal of Grape and Wine Research*, *24*(4), 413–420. https://doi.org/10.1111/ajgw.12349

Christen, D., Schönmann, S., Jermini, M., Strasser, R. J., & Défago, G. (2007). Characterization and early detection of grapevine (Vitis vinifera) stress responses to esca disease by in situ chlorophyll fluorescence and comparison with drought stress. *Environmental and Experimental Botany*, *60*(3), 504–514. https://doi.org/10.1016/j.envexpbot.2007.02.003

Cohen, B., Edan, Y., Levi, A., & Alchanatis, V. (2022). Early Detection of Grapevine (Vitis vinifera) Downy Mildew (Peronospora) and Diurnal Variations Using Thermal Imaging. *Sensors*, *22*(9). https://doi.org/10.3390/s22093585

Cubero, S., Diago, M. P., Blasco, J., Tardaguila, J., Prats-Montalbán, J. M., Ibáñez, J., et al. (2015). A new method for assessment of bunch compactness using automated image analysis. *Australian Journal of Grape and Wine Research*, *21*(1), 101–109. https://doi.org/10.1111/ajgw.12118

Elad, Y. (2016). *Botrytis-the Fungus, the Pathogen and its Management in Agricultural Systems*. https://doi.org/10.1007/978-3-319-23371-0

Elmer, P. A.G., & Reglinski, T. (2006, April). Biosuppression of Botrytis cinerea in grapes. *Plant Pathology*. https://doi.org/10.1111/j.1365-3059.2006.01348.x

Elmer, Philip A G, & Michailides, T. J. (2007). *CHAPTER 14 EPIDEMIOLOGY OF BOTRYTIS CINEREA IN ORCHARD AND VINE CROPS*.

Extension Service, N. (2015). *Growing Grapes in North Dakota: A Guide for Home Gardeners and Hobby Growers (H1761)*. www.ag.ndsu.edu

Fastellini, G., & Schillaci, C. (2020). Precision farming and IoT case studies across the world. In *Agricultural Internet of Things and Decision Support for Precision Smart Farming* (pp. 331–415). Elsevier Inc. https://doi.org/10.1016/B978-0-12-818373-1.00007-X

Fedorina, J., Tikhonova, N., Ukhatova, Y., Ivanov, R., & Khlestkina, E. (2022, February 1). Grapevine Gene Systems for Resistance to Gray Mold Botrytis cinerea and Powdery Mildew Erysiphe necator. *Agronomy*. MDPI. https://doi.org/10.3390/agronomy12020499

Fermaud Villenave d'Orono France.), M. (INRA. (1998). Cultivar susceptibility of grape berry clusters of larvae of Lobesia botrana (Lepidoptera: Tortricidae). *Journal of economic entomology (USA)*.

Ferree, D. C., Ellis, M. A., McArtney, S. J., Brown, M. v., & Scurlock, D. M. (2003). Comparison of fungicide, leaf removal and gibberellic acid on development of grape clusters and botrytis bunch rot of 'vignoles' and 'pinot gris.' *Small Fruits Review*, *2*(4), 3–18. https://doi.org/10.1300/J301v02n04_02

Ferreira, J. H. S., & Marais, P. G. (1987). *Effect of Rootstock Cultivar, Pruning Method and Crop Load on Botrytis cinerea Rot of Vitis vinifera cv. Chenin blanc grapes*.

Flaherty, D. L. ; J. F. L. ; K. A. N. ; K. H. ; M. W. J. (1981). Grape Pest Management . *Grape Pest Management* , (9780931876448).

González-Domínguez, E., Caffi, T., Ciliberti, N., & Rossi, V. (2015). A mechanistic model of botrytis cinerea on grapevines that includes weather, vine growth stage, and the main infection pathways. *PLoS ONE*, *10*(10). https://doi.org/10.1371/journal.pone.0140444

Herrero-Huerta, M., González-Aguilera, D., Rodriguez-Gonzalvez, P., & Hernández-López, D. (2015). Vineyard yield estimation by automatic 3D bunch modelling in field conditions. *Computers and Electronics in Agriculture*, *110*, 17–26. https://doi.org/10.1016/J.COMPAG.2014.10.003

Herrero-huerta, M., Tardy, H., Morcillo, A., & Gonzalez-gonzalez, E. (2022). Grape Bunch Architecture by Low-Cost 3D Scanner Grape Bunch Architecture by Low-Cost 3D Scanner, (June).

International Organization of Vine and Wine Intergovernmental (OIV). (2017). Distribution of the world's grapevine varieties. www.oiv.int. Accessed 29 March 2022

International Organization of Vine and Wine Intergovernmental Organization (OIV). (2019). 2019 Statistical Report on World Vitiviniculture. *Statistical Report on World Vitiviniculture*. Accessed 29 March 2022

Jackson, R. (2016). Viticulture. In *Reference Module in Food Science*. Elsevier. https://doi.org/10.1016/b978-0-08-100596-5.02871-7

Kanatas, P., Travlos, I. S., Gazoulis, I., Tataridas, A., Tsekoura, A., & Antonopoulos, N. (2020). Benefits and limitations of decision support systems (DSS) with a special emphasis on weeds. *Agronomy*. MDPI AG. https://doi.org/10.3390/agronomy10040548

Khirade, S. D., & Patil, A. B. (2015). Plant disease detection using image processing. In *Proceedings - 1st International Conference on Computing, Communication, Control and Automation, ICCUBEA 2015* (pp. 768–771). Institute of Electrical and Electronics Engineers Inc. https://doi.org/10.1109/ICCUBEA.2015.153

Latouche, G., Debord, C., Raynal, M., Milhade, C., & Cerovic, Z. G. (2015). First detection of the presence of naturally occurring grapevine downy mildew in the field by a fluorescence-based method. *Photochemical and Photobiological Sciences*, *14*(10), 1807–1813. https://doi.org/10.1039/c5pp00121h

Li, W., Goodchild, M. F., & Church, R. (2013). An efficient measure of compactness for two-dimensional shapes and its application in regionalization problems. *International Journal of Geographical Information Science*, *27*(6), 1227–1250. https://doi.org/10.1080/13658816.2012.752093

Li, W., Goodchild, M. F., & Church, R. L. (n.d.). *An Efficient Measure of Compactness for 2D Shapes and its Application in Regionalization Problems*.

Math, R. K. M., & Dharwadkar, N. v. (2022). Early detection and identification of grape diseases using convolutional neural networks. *Journal of Plant Diseases and Protection*, *129*(3), 521–532. https://doi.org/10.1007/s41348-022-00589-5

Mazzetto, F., Calcante, A., Mena, A., & Vercesi, A. (2010). Integration of optical and analogue sensors for monitoring canopy health and vigour in precision viticulture. *Precision Agriculture*, *11*(6), 636–649. https://doi.org/10.1007/s11119-010-9186-1

Molitor, D, Rothmeier, M., Behr, M., Fischer, S., Hoffmann, L., & Evers, D. (2011). *Crop cultural and chemical methods to control grey mould on grapes*. *Vitis* (Vol. 50).

Molitor, Daniel, Baus, O., Hoffmann, L., & Beyer, M. (2016). Meteorological conditions determine the thermal-temporal position of the annual Botrytis bunch rot epidemic on Vitis vinifera L. cv. Riesling grapes. *Oeno One*, *50*(4), 231–244. https://doi.org/10.20870/oeno-one.2016.50.4.36

Molitor, Daniel, Schultz, M., Friedrich, B., Viret, O., Hoffmann, L., & Beyer, M. (2018). Efficacy of fenhexamid treatments against Botrytis cinerea in grapevine as affected by time of application and meteorological conditions. *Crop Protection*, *110*, 1–13. https://doi.org/10.1016/J.CROPRO.2018.03.007

Oliver, S. T., González-Pérez, A., & Guijarro, J. H. (2019). Adapting models to warn fungal diseases in vineyards using in-field Internet of Things (IoT) nodes. *Sustainability (Switzerland)*, *11*(2). https://doi.org/10.3390/su11020416

Organizzazione delle Nazioni unite per l'alimentazione e l'agricoltura., & International Organisation of Vine and Wine. (2016). *Table and dried grapes*. s.n.].

Palacios, F., Diago, M. P., & Tardaguila, J. (2019). A non-invasive method based on computer vision for grapevine cluster compactness assessment using a mobile sensing platform under field conditions. *Sensors (Switzerland)*, *19*(17). https://doi.org/10.3390/s19173799

Pommer, C. v, Pires, E. J. P., Terra, M. M., & Passos, I. R. S. (1996). Streptomycin-induced seedlessness in the grape cultivar Rubi (Italia Red). *American journal of enology and viticulture*.

Rist, F., Gabriel, D., Mack, J., Steinhage, V., Töpfer, R., & Herzog, K. (2019). Combination of an automated 3D field phenotyping workflow and predictive modelling for high-throughput and non-invasive phenotyping of grape bunches. *Remote Sensing*, *11*(24), 1–22. https://doi.org/10.3390/rs11242953

Robinson, Jancis. (1986). Vines, grapes, and wines, 280. Accessed 31 March 2022

Romanazzi, G., & Feliziani, E. (2014). Botrytis cinerea (Gray Mold). In *Postharvest Decay: Control Strategies* (pp. 131–146). Elsevier Inc. https://doi.org/10.1016/B978-0-12-411552-1.00004-1

Sankaran, S., Mishra, A., Ehsani, R., & Davis, C. (2010, June). A review of advanced techniques for detecting plant diseases. *Computers and Electronics in Agriculture*. https://doi.org/10.1016/j.compag.2010.02.007

Santesteban, L. G. (2019). Precision viticulture and advanced analytics. A short review. *Food Chemistry*, *279*, 58–62. https://doi.org/10.1016/J.FOODCHEM.2018.11.140

Sarri, D., Lisci, R., Rimediotti, M., Vieri, M., & Storchi, P. (2015). Applications of the precision viticulture techniques in the Chianti district. In *1st Conference on Proximal Sensing Supporting Precision Agriculture - Held at Near Surface Geoscience 2015* (pp. 121–125). European Association of Geoscientists and Engineers, EAGE. https://doi.org/10.3997/2214-4609.201413851

Sbpahi, A. (1980). *Estimating duster compactness in Yaghouti grapes*.

S.F. Di Gennaro, P. T. P. C. A. B. A. M. (2019). A precision viticulture UAV-based approach for early yield prediction in vineyard. *Precision agriculture '19*.

Shavrukov, Y. N., Dry, I. B., & Thomas, M. R. (2004). Inflorescence and bunch architecture development in Vitis vinifera L. *Australian Journal of Grape and Wine Research*, *10*(2), 116–124. https://doi.org/10.1111/j.1755-0238.2004.tb00014.x

Staats, M., van Baarlen, P., & van Kan, J. A. L. (2005). Molecular phylogeny of the plant pathogenic genus Botrytis and the evolution of host specificity. *Molecular Biology and Evolution*, *22*(2), 333–346. https://doi.org/10.1093/molbev/msi020

Sternad Lemut, M., Sivilotti, P., Butinar, L., & Vrhovšek, U. (2010). *Controlling microbial infection by managing grapevine canopy*.

Stummer Belinda, Dambergs Bob, & Scott Eileen. (2007). *Application of NIR for disease assessment*.

Sturges, H. A. (1926). The Choice of a Class Interval. *Journal of the American Statistical Association*, *21*(153), 65–66. https://doi.org/10.1080/01621459.1926.10502161

Tardaguila, J., Stoll, M., Gutiérrez, S., Proffitt, T., & Diago, M. P. (2021). Smart applications and digital technologies in viticulture: A review. *Smart Agricultural Technology*, *1*, 100005. https://doi.org/10.1016/j.atech.2021.100005

Tello, J, & Ibáñez, J. (2014). *Evaluation of indexes for the quantitative and objective estimation of grapevine bunch compactness*. *Vitis* (Vol. 53).

Tello, J., & Ibáñez, J. (2018, January 1). What do we know about grapevine bunch compactness? A state-of-the-art review. *Australian Journal of Grape and Wine Research*. Blackwell Publishing Ltd. https://doi.org/10.1111/ajgw.12310

Tello, Javier, Cubero, S., Blasco, J., Tardaguila, J., Aleixos, N., & Ibáñez, J. (2016). Application of 2D and 3D image technologies to characterise morphological attributes of grapevine clusters. *Journal of the science of food and agriculture*, *96*(13), 4575–4583. https://doi.org/10.1002/jsfa.7675

Towsend, G. R. H. J. W. (1943). Methods for estimating losses caused by disease in fungicide experiments. *PLANT DISEASE REPORTER*, *v.27(17)*, 340-343,.

Tugnolo, A., Giovenzana, V., Beghi, R., Brancadoro, L., & Guidetti, R. (2017). *APPLICATION OF VISIBLE/NEAR INFRARED SPECTROSCOPY TO ASSESS THE GRAPE INFECTION AT THE WINERY*.

Underhill, A., Hirsch, C., & Clark, M. (2020). Image-based phenotyping identifies quantitative trait loci for cluster compactness in grape. *Journal of the American Society for Horticultural Science*, *145*(6), 363–373. https://doi.org/10.21273/JASHS04932-20

Unione Italiana Vini. (2020, February 3). https://corrierevinicolo.unioneitalianavini.it/. *Unione Italiana Vini*. https://corrierevinicolo.unioneitalianavini.it/

Valdés-Gómez, H., Fermaud, M., Roudet, J., Calonnec, A., & Gary, C. (2008). Grey mould incidence is reduced on grapevines with lower vegetative and reproductive growth. *Crop Protection*, *27*(8), 1174–1186. https://doi.org/10.1016/j.cropro.2008.02.003

Vanderweide, J., Frioni, T., Ma, Z., Stoll, M., Poni, S., & Sabbatini, P. (2020). Early leaf removal as a strategy to improve ripening and lower cluster rot in cool climate (Vitis vinifera l.) pinot grigio. *American Journal of Enology and Viticulture*, *71*(1), 70–79. https://doi.org/10.5344/ajev.2019.19042

Veneto Agricoltura. (2019). VENETO VINEYARD, STILL GROWING... – Veneto Agriculture. https://www.venetoagricoltura.org/2019/12/news/vigneto-veneto-cresce-ancora/. Accessed 23 April 2022

Vin, O. I. de la V. et du. (2009). *OIV descriptor list for grape varieties and Vitis species*. Paris, France.

Wegher, M., Faralli, M., & Bertamini, M. (2022). Cluster-Zone Leaf Removal and GA 3 Application at Early Flowering Reduce Bunch Compactness and Yield per Vine in Vitis vinifera cv. Pinot Gris. https://doi.org/10.3390/horticulturae8010081

Wirth, M. A. (2004). *Shape Analysis & Measurement*.

Xu, H. R., Ying, Y. B., Fu, X. P., & Zhu, S. P. (2007). Near-infrared Spectroscopy in detecting Leaf Miner Damage on Tomato Leaf. *Biosystems Engineering*, *96*(4), 447–454. https://doi.org/10.1016/j.biosystemseng.2007.01.008

Yamasaki, Y., Morie, M., & Noguchi, N. (2022). Development of a high-accuracy autonomous sensing system for a field scouting robot. *Computers and Electronics in Agriculture*, *193*. https://doi.org/10.1016/j.compag.2021.106630

Yang, C. (2020, May 1). Remote Sensing and Precision Agriculture Technologies for Crop Disease Detection and Management with a Practical Application Example. *Engineering*. Elsevier Ltd. https://doi.org/10.1016/j.eng.2019.10.015

Zhang, D., & Lu, G. (2004). Review of shape representation and description techniques. *Pattern Recognition*, *37*(1), 1–19. https://doi.org/10.1016/j.patcog.2003.07.008

Zhang, J., Huang, Y., Pu, R., Gonzalez-Moreno, P., Yuan, L., Wu, K., & Huang, W. (2019, October 1). Monitoring plant diseases and pests through remote sensing technology: A

review. *Computers and Electronics in Agriculture*. Elsevier B.V. https://doi.org/10.1016/j.compag.2019.104943